

# An extracellular Zn-only superoxide dismutase from *Puccinia striiformis* confers enhanced resistance to host-derived oxidative stress

Jie Liu,<sup>1†</sup> Tao Guan,<sup>1†</sup> Peijing Zheng,<sup>1†</sup>  
Liyang Chen,<sup>1</sup> Yang Yang,<sup>1</sup> Baoyu Huai,<sup>1</sup> Dan Li,<sup>1</sup>  
Qing Chang,<sup>2</sup> Lili Huang<sup>2</sup> and Zhensheng Kang<sup>2\*</sup>

<sup>1</sup>State Key Laboratory of Crop Stress Biology for Arid Areas and College of Life Sciences, Northwest A&F University, Yangling, People's Republic of China.

<sup>2</sup>State Key Laboratory of Crop Stress Biology for Arid Areas and College of Plant Protection, Northwest A&F University, Yangling, People's Republic of China.

## Summary

**Accumulation of reactive oxygen species (ROS) following plant-pathogen interactions can trigger plant defence responses and directly damage pathogens. Thus, it is essential for pathogens to scavenge host-derived ROS to establish a parasitic relationship. However, the mechanisms protecting pathogens from host-derived oxidative stress remain unclear. In this study, a superoxide dismutase (SOD) gene, *PsSOD1*, was cloned from a wheat–*Puccinia striiformis* f. sp. *tritici* (*Pst*) interaction cDNA library. Transcripts of *PsSOD1* were up-regulated in the early infection stage. Heterologous mutant complementation and biochemical characterization revealed that *PsSOD1* encoded a Zn-only SOD. The predicted signal peptide was functional in an invertase-mutated yeast strain. Furthermore, immunoblot analysis of apoplastic proteins in *Pst*-infected wheat leaves and bimolecular fluorescence complementation suggested that *PsSOD1* is a secreted protein that potentially forms a dimer during *Pst* infection. Overexpression of *PsSOD1* enhanced *Schizosaccharomyces pombe* resistance to exogenous superoxide. Transient expression of *PsSOD1* in *Nicotiana benthamiana* suppressed Bax-induced cell death. Knockdown of *PsSOD1* using a host-induced gene silencing (HIGS) system reduced the virulence of *Pst*, which was**

**associated with ROS accumulation in HIGS plants. These results suggest that *PsSOD1* is an important pathogenicity factor that is secreted into the host-pathogen interface to contribute to *Pst* infection by scavenging host-derived ROS.**

## Introduction

Reactive oxygen species (ROS) are by-products of cellular respiration and include superoxide anion (O<sub>2</sub><sup>-</sup>), hydroxyl radicals (·OH) and hydrogen peroxide (H<sub>2</sub>O<sub>2</sub>) (Mittler, 2002). These unstable molecules are produced both as a result of normal aerobic metabolic processes inside the plant cell and in response to abiotic stresses, including drought, heat, high salinity, highlight, osmotic stress and metal toxicity (Perez and Brown, 2014). ROS are also produced and play important roles during pathogenic invasion. ROS are key signalling molecules that trigger a variety of plant defence responses to control or clear pathogen infection (Apel and Hirt, 2004). Additionally, these species can cause direct damage to macromolecules, such as DNA, proteins, and lipids, on or in the pathogens, leading to pathogen death (Fridovich, 1978; Imlay, 2003). Because ROS are highly toxic to pathogens, it is necessary for effective pathogens to scavenge host-derived ROS to establish parasitic relationships.

Superoxide dismutases (SODs, EC 1.15.1.1) constitute the first line of cellular defences against ROS damages that catalyse the conversion of superoxide anions to molecular oxygen and hydrogen peroxide (Fridovich, 1995). These enzymes are widely expressed in prokaryotic and eukaryotic cells and generally utilize metal ions as cofactors. To date, four types of SODs with different metal cofactors have been reported: manganese SOD (Mn-SOD), iron SOD (Fe-SOD), copper/zinc SOD (Cu/Zn-SOD), and nickel SOD (Ni-SOD) (Abreu and Cabelli, 2010; Perry *et al.*, 2010). The number, type, and localization of SOD isozymes vary with the species, developmental stage, and environmental stress conditions. Mn-SOD and Fe-SOD are closely related; their protein structures differ from the other two groups, and they were recently assigned to one family. Mn-SOD and Fe-SOD are prevalent in prokaryotes, mitochondria and chloroplasts

Received 2 May, 2016; accepted 5 July, 2016. \*For correspondence. E-mail: kangzs@nwsuaf.edu.cn; Tel. (+86) 0298 7080061; Fax (+86) 0298 7080061. †These authors contributed equally to this work.

of eukaryotes and likely evolved from a common ancestor (Miller, 2012). Cu/Zn-SODs are found in some bacteria and in the cytosol of eukaryotes, including yeast, mammals and plants (Pilon *et al.*, 2011). In plants, Cu/Zn-SOD is also localized to the peroxisomes and plastids (Myouga, *et al.*, 2008). Ni-SOD has only been found in streptomycetes (Wuerges, *et al.*, 2004) and cyanobacteria thus far (Priya *et al.*, 2007).

The fungal SODs identified to date have Cu/Zn or Mn cofactors and are predominantly found in the cytosol or mitochondria. Several Mn-SODs are involved in the survival and the resistance of aerobic fungi to multiple stresses. Knocking out a Mn-SOD gene from *Schizosaccharomyces cerevisiae* results in rapid death in the stationary phase (Longo *et al.*, 1999) and increases susceptibility to oxidative stress (O'Brien *et al.*, 2004). The Mn-SOD mutants of *Schizosaccharomyces pombe* are more sensitive to various stresses than wild-type strains (Jeong *et al.*, 2001). In addition, Mn-SODs have also been identified as virulence factors of many fungal pathogens. For example, a mitochondrial Mn-SOD SOD2 is required for *Cryptococcus neoformans* virulence to mice (Narasipura *et al.*, 2005). Xie *et al.* (2012) also found that BbSOD2, a cytosolic Mn-SOD, contributes significantly to the virulence and stress tolerance of *Beauveria bassiana*.

Cu/Zn-SODs are the main contributors to cytosolic SOD activity. Currently, Cu/Zn-SODs are divided into two classes. One type contains intracellular, largely cytosolic Cu/Zn-SODs, and the other group consists of extracellular Cu/Zn SODs (EC-SODs). EC-SODs are either secreted from cells or attached to the cell wall by a glycosylphosphatidylinositol (GPI) anchor with a putative omega site at specific residues (Gleason *et al.*, 2014). Numerous studies have indicated that Cu/Zn-SODs play central roles in fungal growth, pathogenesis and resistance to oxidative stress. For example, *Saccharomyces cerevisiae* and *Candida glabrata* lacking SOD1 (a cytosolic Cu/Zn-SOD) both show obvious growth defects and increased sensitivity to redox-cycling drugs, such as menadione (Manfredini *et al.*, 2004; Briones-Martindel-Campo *et al.* 2015). In *Candida albicans*, a SOD1 knockout (a cytosolic Cu/Zn-SOD) exhibits attenuated virulence in an animal model of systemic infection (Hwang *et al.*, 2002; Chaves *et al.*, 2007) and is more susceptible to killing by macrophages (Hwang *et al.*, 2002) and polymorphonuclear neutrophils (PMNs) (Chaves *et al.*, 2007). In addition, a GPI-anchored protein, SOD5 (an EC-SOD) from *C. albicans*, is essential for pathogen defence and has been shown to be critical for combating the oxidative burst of infection (Gleason *et al.*, 2014). The fungal pathogen *Histoplasma capsulatum* EC-SOD SOD3 facilitates *Histoplasma* pathogenesis by detoxifying host-derived ROS, promoting *Histoplasma* survival (Youseff *et al.*, 2012).

Wheat stripe rust is one of the most serious diseases of wheat worldwide. This disease can cause wheat yield losses and pose a threat to food security. *Puccinia*

*striiformis* f. sp. *tritici* (*Pst*), the causal agent of wheat stripe rust, is an obligate biotrophic fungus with a complex life cycle and a series of highly specialized infection structures. The host-pathogen interaction is accompanied by changes in ROS. Previous studies have found an accumulation of  $O_2^-$  and  $H_2O_2$  at infection sites in the incompatible interaction between wheat and *Pst*, but ROS could not be detected in the compatible interaction (Wang *et al.*, 2007). However, little information is available regarding ROS clearance in the wheat-*Pst* interaction. In this study, a *Pst* SOD gene (*PsSOD1*) that was significantly up-regulated in the early infection stage was isolated, and characterized using heterologous expression. Secretion of PsSOD1 was determined during *Pst* infection of wheat. In addition, overexpression and knockdown of *PsSOD1* were performed to identify its functions in the wheat-*Pst* interaction. Our results indicate that *PsSOD1* contributed to *Pst* infection of wheat by protecting *Pst* from host-derived oxidative stress.

## Results

### PsSOD1 encodes a Zn-only SOD

A cDNA containing a full-length gene orthologous to SOD, designated *PsSOD1*, was isolated from a previously described cDNA library (Ma *et al.*, 2009). Subsequently, the 1062-bp full-length cDNA was obtained using RT-PCR. The open reading frame (ORF) of *PsSOD1* consists of 612 nucleotides and is predicted to encode a polypeptide of 203 amino acids with a calculated molecular mass of 21,802 Da, an isoelectric point (pI) of 8.94, and a Cu/Zn-SOD domain. Interestingly, PsSOD1 only contains  $Zn^{2+}$  binding sites (H111, T119, E135, and D138) and lacks  $Cu^{2+}$  binding sites, which indicates that PsSOD1 is not a traditional Cu/Zn-SOD enzyme (Supporting Information Fig. S1A). In addition, signal peptide prediction using SignalP 4.1 revealed that PsSOD1 is likely a secreted protein (Supporting Information Fig. S1B).

The 203 amino acid sequence was used as a query sequence to search the most up-to-date databases. Homologous proteins from other fungi with the highest similarities to PsSOD1 were identified. The protein sequence showed 56% identity with Cu/Zn-SOD from *Puccinia graminis* f. sp. *tritici* CRL 75-36-700-3 (GenBank accession number XP\_003326013), 45% identity with Cu/Zn-SOD from *Melampsora larici-populina* 98AG31 (GenBank accession number XP\_007413252), and 34% identity with Cu/Zn-SOD from *Puccinia sorghi* (GenBank accession number KNZ59826). The phylogenetic analysis of PsSOD1 with homologous proteins from other fungi revealed that PsSOD1 displays greater similarity to Cu/Zn-SODs from basidiomycetous fungi, especially rust fungi, compared with those from ascomycetous fungi (Fig. 1A).

The alignment of PsSOD1 with the three aforementioned Cu/Zn-SODs from other rust fungi is shown in

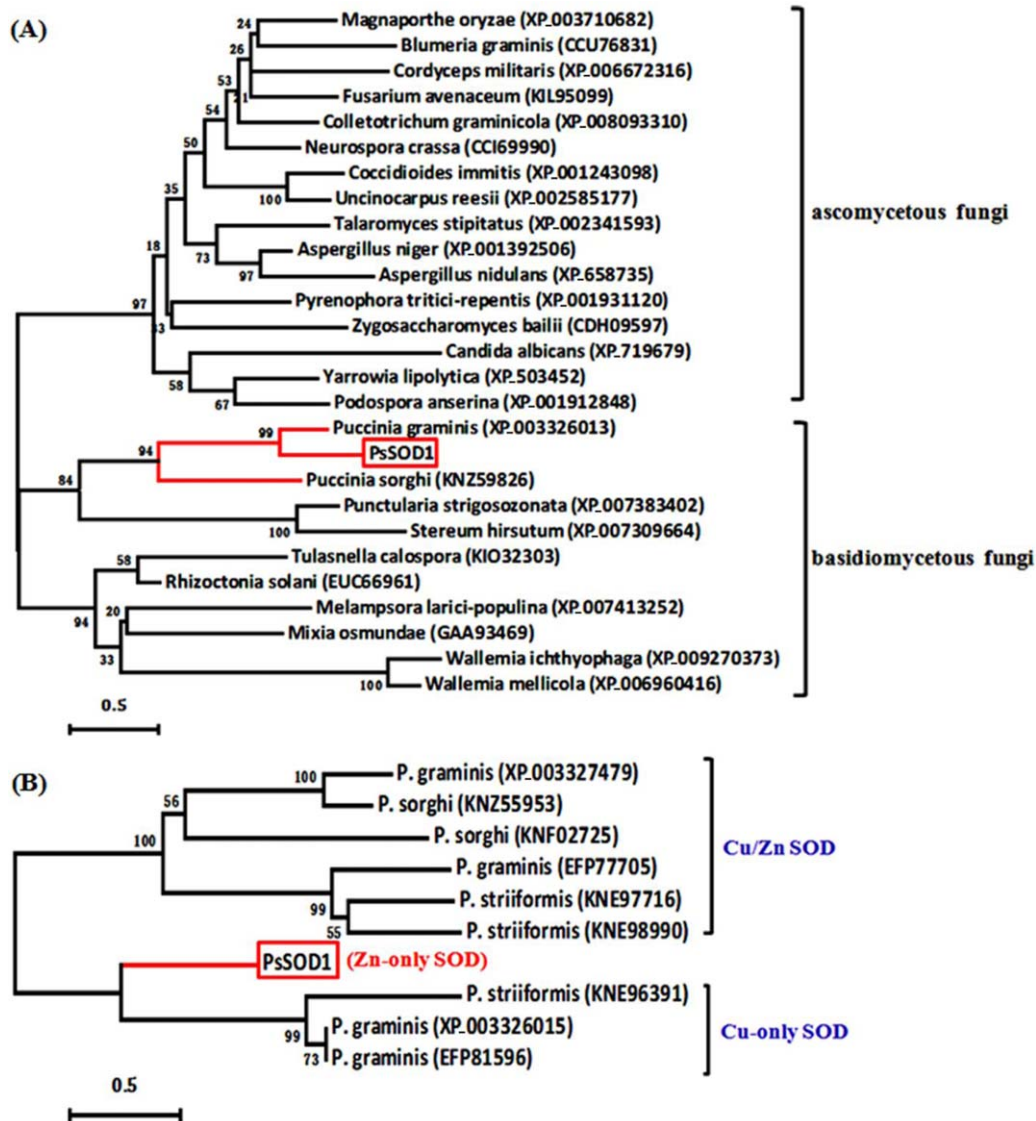


**Fig. 1.** Phylogenetic analysis of PsSOD1 and selected homologous proteins from other fungi (A) and rust fungi (B). The unrooted phylogram was constructed based on the NJ method. The confidence level for the groupings was estimated using 1000 bootstrap replicates. The numbers adjacent to the branch points indicate the percentage of replicates supporting each branch.

Supporting Information Fig. S2, displaying significant interspecies variations in the amino acid sequences. Further analysis revealed that homologous proteins of PsSOD1 shown in Fig. 1A contained both  $\text{Cu}^{2+}$  and  $\text{Zn}^{2+}$  binding sites (Supporting Information Fig. S3A), or only had  $\text{Cu}^{2+}$  binding sites (Supporting Information Fig. S3B), which were different from PsSOD1. Thus, *PsSOD1* might encode a novel SOD. In addition, genome databases of some representative rust fungi (including *Uromyces*, *Puccinia*, and *Melampsora*) were investigated. The results showed that PsSOD1-like proteins are only present in the stripe rust fungi genome, and other rust fungi do not contain Zn-only SODs. The phylogenetic relationships of PsSOD1 with

homologous proteins (Cu/Zn-SODs and Cu-only SODs) from other rust fungi also revealed that PsSOD1 is separated into a new SOD branch (Fig. 1B). These results indicate that PsSOD1 may be a novel SOD that is specific to stripe rust fungi.

#### *PsSOD1 is conserved between Pst isolates*

To identify intraspecies polymorphisms in *PsSOD1*, we compared the coding regions of five sequenced *Pst* isolates, including a Chinese isolate (CYR32), three US isolates (PST21, PST78 and PST130) and a UK isolate (PST87-7). Compared with the PsSOD1 sequence from

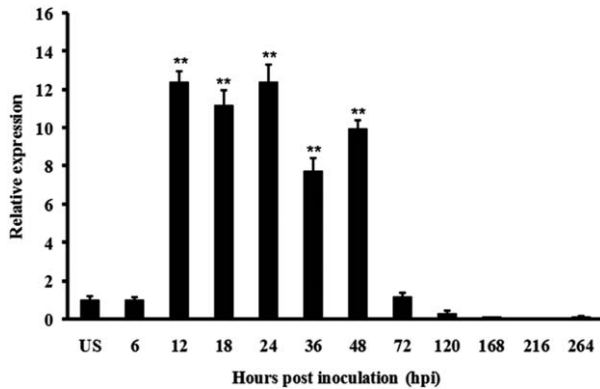


**Fig. 2.** Transcript levels of *PsSOD1* at various stages of *Pst* infection of Su11.

The expression levels of *PsSOD1* were calculated by the comparative Ct method with *EF-1* in *Pst* as an internal standard. Relative quantifications are compared with the expression levels of nongerminated urediniospores. The means and standard errors were calculated from three replicates. US, urediniospores; Bars indicate the standard deviation of the mean; double asterisks indicate  $P < 0.01$ .

CYR32, which is one of the predominant *Pst* isolates in China, only three nucleotide substitutions were observed among the five *Pst* isolates, including two synonymous substitutions and one non-synonymous substitution (Supporting Information Table S1). In addition, the only mutation is not in the SOD domain or the Zn binding sites of *PsSOD1* (Supporting Information Fig. S4). A gene (less than five nucleotide substitutions between lineages) is generally considered to be conserved (Wang *et al.*, 2011). Thus, *PsSOD1* is conserved between *Pst* isolates.

#### *PsSOD1* is up-regulated during *Pst* infection of wheat

The *PsSOD1* transcript levels were measured at different developmental stages during *Pst* infection by quantitative reverse transcription PCR (qRT-PCR). *PsSOD1* was expressed in ungerminated urediniospores and infected wheat tissues harvested from 6 to 264 h postinoculation (hpi). In ungerminated urediniospores, *PsSOD1* transcripts were detected at relatively low levels. However, the expression of *PsSOD1* was sharply up-regulated at 12 hpi and remained constant until 2 days postinoculation (dpi) (Fig. 2). During the later stages of infection in wheat, the expression level of *PsSOD1* was extremely low (Fig. 2). These results indicate an in-planta induction of *PsSOD1* in the early stage of *Pst* infection.

#### *PsSOD1* largely complements the *S. cerevisiae* SOD1 mutant

To identify the function of *PsSOD1* in *S. cerevisiae*, pDR195 and pDR195-*PsSOD1* were transformed into a *S. cerevisiae*

*SOD1* mutant with obvious growth defects under aerobic conditions. Numerous transformants were obtained on synthetic complete (SC) media without uracil, and they were confirmed by PCR analysis and then sequenced. The transformants displayed identical phenotypes, although only data from transformant CS-1 are presented below.

The growth curves of the *S. cerevisiae* *SOD1* mutant carrying the empty pDR195 vector and the complemented strain CS-1 were monitored in SC media containing glucose or ethanol as the sole carbon source. The results showed a clear increase in the growth rate of the complemented strain CS-1 compared with the *S. cerevisiae* *SOD1* mutant carrying the empty pDR195 vector in SC media with glucose (Fig. 3A). In SC media with ethanol, similar results were observed (Fig. 3B). In addition, the sensitivity of the complemented strain CS-1 to menadione was assayed. As shown in Fig. 3C, the CS-1 strain displayed increased resistance to menadione compared with the control. These results indicate that the expression of the *PsSOD1* gene in *S. cerevisiae* largely complements the defects observed in the *SOD1* mutant.

#### Biochemical characterization of *PsSOD1*

The recombinant *PsSOD1* was expressed as a soluble protein in cultures of *Escherichia coli* BL21(DE3)plysS transformed with the plasmid pGEX4T-1-*PsSOD1* following induction by 1 mM IPTG, as shown in the SDS-PAGE profiles (Fig. 4A). The GST-tagged protein was purified to a single protein band by one-step chromatography. The electrophoretic mobility of the expressed GST-*PsSOD1* fusion protein was consistent with the predicted molecular weight of approximately 46 kDa (Fig. 4A).

Biochemical characterization of *PsSOD1* was then performed. The optimum temperature was approximately 20°C. Higher temperatures resulted in a rapid loss of enzymatic activity (Fig. 4B). The pH optimum was determined to be approximately pH 9.0 (Fig. 4C). In addition, metal cations also showed differential effects on the enzymatic activity of *PsSOD1*. Inclusion of 0.5 mM  $Zn^{2+}$  in the reaction enhanced the enzymatic activity by 85% (Fig. 4D). Addition of  $Cu^{2+}$  did not result in obvious changes in enzymatic activity (Fig. 4D), which is consistent with the bioinformatics prediction of *PsSOD1*. Furthermore, the enzymatic activity of *PsSOD1* was inhibited by  $Fe^{3+}$  and  $Mn^{2+}$  to some extent (Fig. 4D).

#### *PsSOD1* is secreted into the apoplastic fluids of wheat and potentially forms dimers

To functionally validate the SignalP 4.1 predictions, the signal peptide of *PsSOD1* was tested using a genetic assay based on the requirement of yeast cells for invertase secretion to grow on raffinose media. As a negative

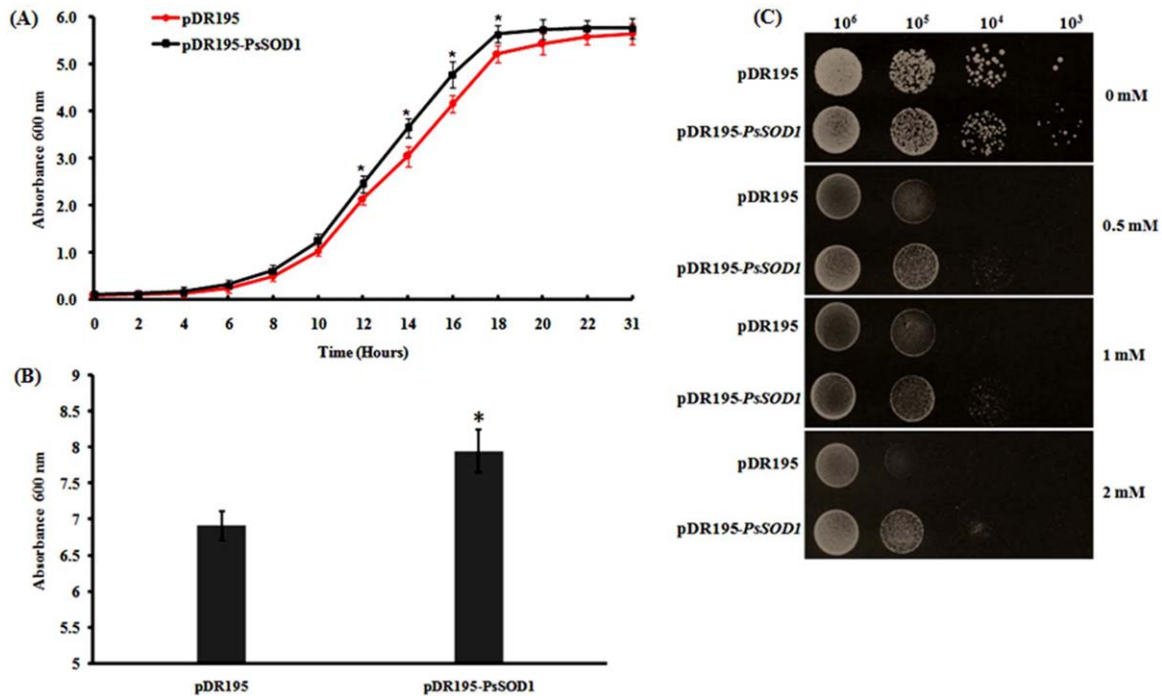


**Fig. 3.** Growth of the *S. cerevisiae* strains under different conditions.

A. The *SOD1* mutant carrying the empty vector pDR195 and the complemented strain (CS-1) carrying the recombinant plasmid pDR195-*PsSOD1* were grown in SC media with 2% glucose, and  $OD_{600}$  was measured at the indicated times. Cells were grown with shaking in flasks to achieve normal aeration.

B. The *SOD1* mutant with pDR195 and CS-1 were grown in 2% ethanol. Flasks were inoculated at an initial  $OD_{600}$  of 0.01. The data shown were obtained at 90 h during the normal aeration experiment.

C. Colonies of the *SOD1* mutant with pDR195 and CS-1 were grown on SC media containing 0 (control), 0.5, 1, and 2 mM menadione. All experiments were repeated three times. Asterisks indicate a significant difference ( $P < 0.05$ ) compared with the control using Student's *t*-test.

control, we tested the N-terminus of the *Magnaporthe oryzae* homologue Mg87, which was not predicted to be secreted. The secretory leader of Avr1b was used as a positive control. The results showed that both the PsSOD1 and Avr1b fused constructs enabled the invertase mutated yeast strain to grow on CMD-W media (yeast can grow without invertase secretion) and YPRAA media (yeast can grow only when invertase is secreted) (Fig. 5A). However, when the Mg87 N-terminus was fused to the truncated invertase, the transformed yeast strains did not grow on YPRAA plates (Fig. 5A). These results confirmed that the signal peptide of PsSOD1 was functional, but the N-terminus of Mg87 was not, which was consistent with the predictions of SignalP 4.1 (Fig. 5A).

Cu/Zn-SOD generally exists as a polymer (Zeinali *et al.*, 2015). To confirm secretion and polymerization of PsSOD1 during *Pst* infection of wheat, apoplastic proteins from uninfected and *Pst*-infected wheat leaves were separated by native PAGE and immunoblotted with an anti-PsSOD1 antibody. The Western blot results for apoplastic proteins from *Pst*-infected and uninfected leaves revealed clear differences. For apoplastic proteins from *Pst*-infected leaves,

the specific band (approximately 40 kDa) was observed (Fig. 5B), and the molecular weight was approximately two times higher than that of the PsSOD1 monomer. However, the antibody did not bind to proteins in the apoplastic proteins from uninfected wheat leaves (Fig. 5B). For the positive control, consistent with the native-PAGE results shown in Supporting Information Fig. S5A, the GST-PsSOD1 fusion proteins were clearly observed by the presence of a band of approximately 46 kDa (Fig. 5B), indicating GST-PsSOD1 fusion proteins could not form dimers in spite of dimerization of GST itself (Supporting Information Fig. S5A). In addition, when apoplastic proteins from *Pst*-infected leaves were separated in the SDS-PAGE gels and immunoblotted, the specific band similar to the PsSOD1 monomer in molecular weight appeared (Supporting Information Fig. S5B). Thus, we concluded that PsSOD1 likely forms dimers when it is secreted into the host.

To confirm the oligomerization of PsSOD1, interactions between PsSOD1 were tested by in planta bimolecular fluorescence complementation (BiFC) experiments in transiently transformed *Nicotiana benthamiana* leaves. The results showed that strong fluorescence signals were

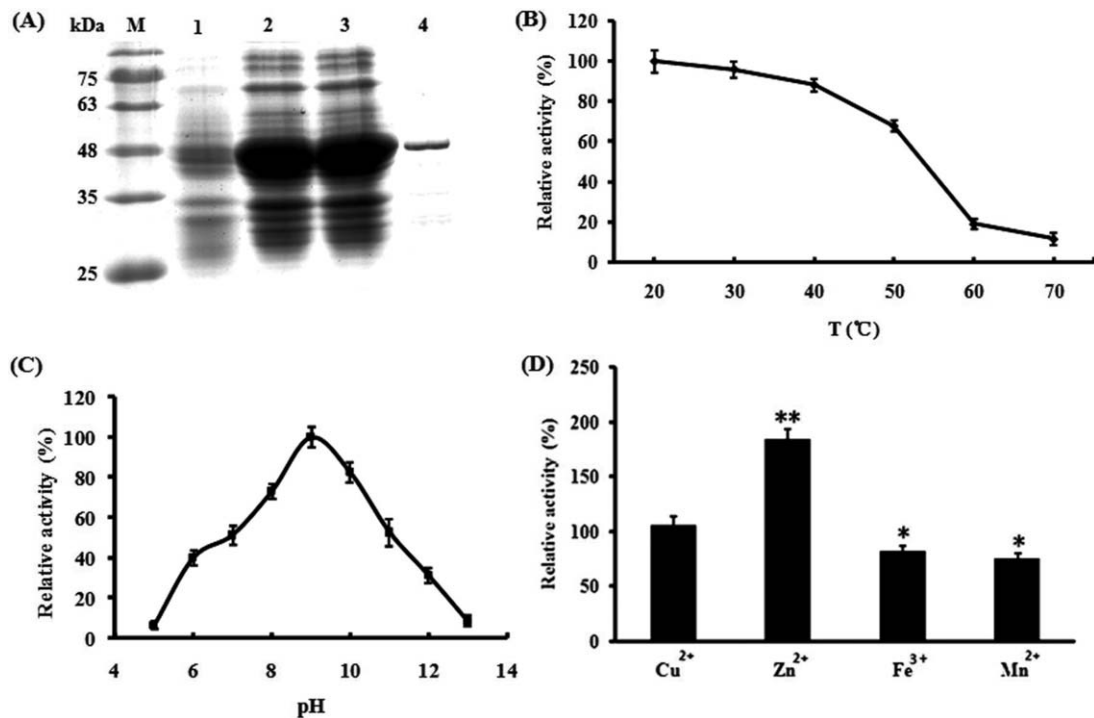


**Fig. 4.** Purification and biochemical characterization of PsSOD1 expressed in *E. coli* BL21(DE3)plysS.

A. The SDS-PAGE profiles of PsSOD1 expressed in *E. coli* BL21(DE3)plysS. Lane 1, uninduced *E. coli* cell lysates harbouring pGEX4T-1-*PsSOD1*; lane 2, *E. coli* cell lysates harbouring pGEX4T-1-*PsSOD1* induced by IPTG; lane 3, soluble fractions from the cell culture expressing PsSOD1; lane 4, purified GST-PsSOD1 proteins; M, marker.

B and C. Thermal and pH stability of the purified PsSOD1.

D. Effects of metal ions on the activity of the purified PsSOD1. Asterisks indicate a significant difference ( $P < 0.05$ ) compared with the control using Student's *t*-test.

observed when agrobacteria carrying pSPYNE(R)173-*PsSOD1* or pSPYCE(M)-*PsSOD1* were co-infiltrated into *N. benthamiana* leaves (Fig. 5C). However, no fluorescence was observed when agrobacteria containing pSPYNE(R)173-*PsSOD1* or the empty vector pSPYCE(M) was co-infiltrated (Fig. 5C), indicating that PsSOD1 might interact with itself and form dimers.

#### Overexpression of PsSOD1 enhances stress resistance

To determine the role of *PsSOD1* in scavenging exogenous superoxide, *S. pombe* cells carrying the recombinant plasmid pREP41-*PsSOD1* were challenged in vitro with superoxide. To generate superoxide in vitro, increasing amounts of xanthine oxidase were added to *S. pombe* suspensions in Tris buffer with excess hypoxanthine; the amount of superoxide proportionally increases with the concentration of xanthine oxidase enzyme (data not shown). The results showed that the survival of the *S. pombe* strain containing the recombinant plasmid pREP41-*PsSOD1* following the superoxide challenge was significantly increased compared with the control strain carrying the empty pREP41 plasmid (Fig. 6A), indicating

that extracellular PsSOD1 may protect *S. pombe* from exogenous superoxide.

In addition, to investigate whether *PsSOD1* functions in suppressing the host defence responses, *PsSOD1* was overexpressed in tobacco using potato virus X (PVX) delivery in combination with Bax, a pro-apoptotic protein from mouse that triggers a hypersensitive response (HR)-like cell death response in plants. When *N. benthamiana* leaves were infiltrated with *Agrobacterium tumefaciens* strains individually carrying PVX-*PsSOD1*, empty vector, or MgCl<sub>2</sub>, no cell death was observed (Fig. 6B; circle 1, 4 and 6); tobacco leaves infiltrated with Bax + *PsSOD1* (Fig. 6B; circle 2) or Bax only (Fig. 6B; circle 5) both showed a similar cell death phenotype (after 5 days). However, when *PsSOD1* was infiltrated prior to Bax for 24 h, cell death was significantly suppressed (Fig. 6B; circle 3).

To confirm that *PsSOD1* and *Bax* were successfully expressed in *N. benthamiana* leaves infiltrated by *A. tumefaciens* carrying different vectors, RT-PCR was performed. As shown in Fig. 6C, *PsSOD1* and *Bax* were both detected after infiltration, either alone or in combination. However, they were not detected after treatment with the empty vector or MgCl<sub>2</sub>. These results indicate that PsSOD1 is related to cell death suppression.

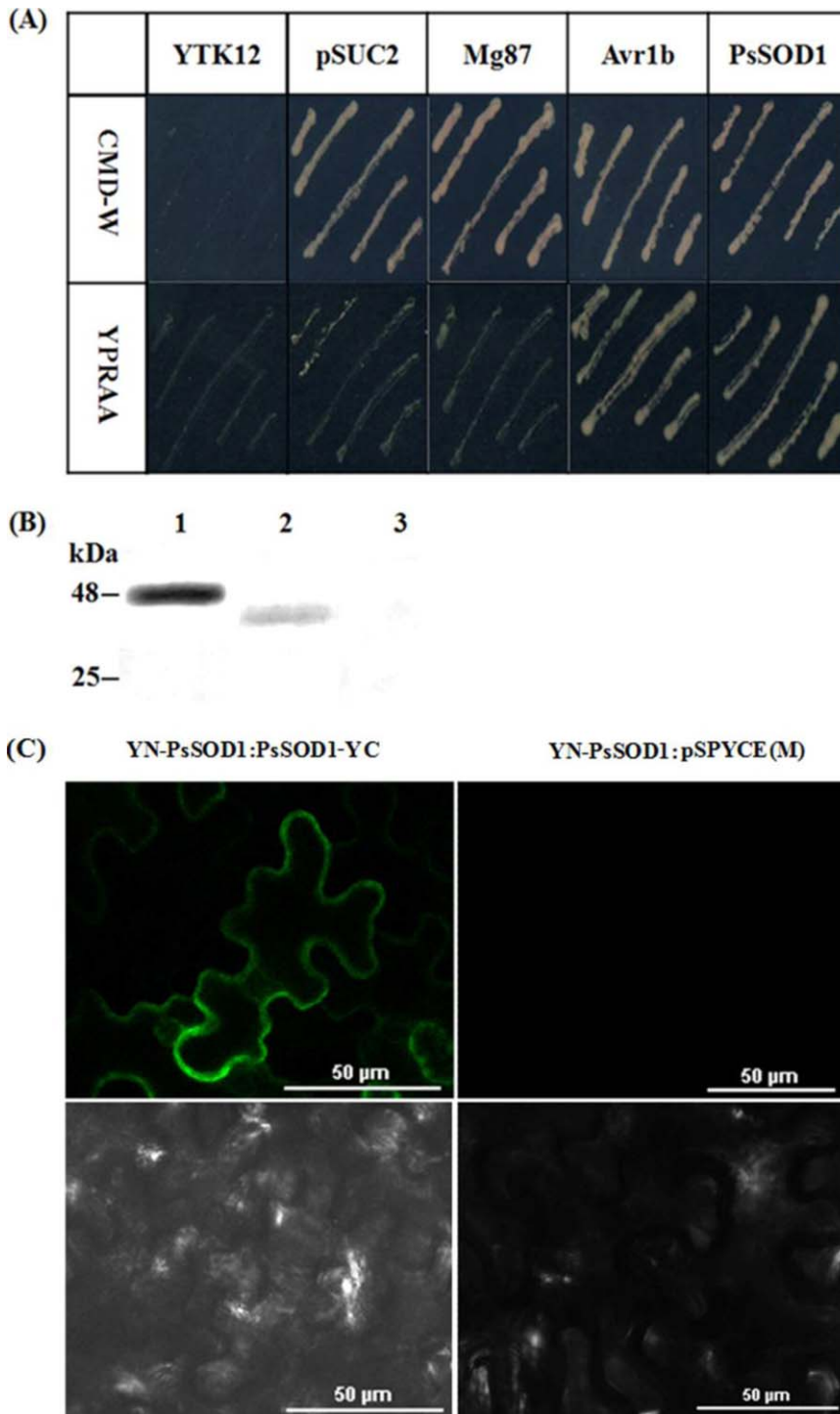


**Fig. 5.** A. Functional validation of the signal peptide of PsSOD1.

The PsSOD1 or Avr1b signal peptides or the first 25 amino acids of Mg87 were fused in-frame to the invertase sequence in the pSUC2 vector and transformed into the yeast YTK12 strain. Controls include the untransformed YTK12 strain and YTK12 carrying the pSUC2 vector. Strains that are unable to secrete invertase can grow on CMD-W medium but not on YPRAA medium.

B. Western blot analysis of the apoplastic proteins separated in the native PAGE gels. Lane 1, GST-PsSOD1 fusion proteins; lane 2, apoplastic proteins from *Pst*-infected wheat leaves; lane 3, apoplastic proteins from healthy wheat leaves.

C. PsSOD1 interacts with itself in *N. benthamiana*. Microscopic analysis of BiFC complexes formed by the indicated plasmid combinations after 3 days of infiltration in *N. benthamiana* leaves.

#### *Silencing of PsSOD1 by HIGS reduces the virulence of Pst in wheat*

Currently, there is no effective transformation system for rust fungi; thus, the HIGS technique mediated by BSMV was used to knockdown the expression of *PsSOD1* in *Pst*. All BSMV-inoculated plants displayed mild chlorotic mosaic symptoms at 9 days postinoculation (dpi), and no obvious

defects were observed during subsequent growth (Fig. 7A). In the *TaPDS*-silenced plants, a bleaching phenotype was observed at 15 dpi (Fig. 7A), indicating that the BSMV-HIGS system functioned correctly. The fourth leaves of the wheat plants were inoculated with CYR32, and the rust disease phenotypes were photographed at 15 dpi. Wheat leaves inoculated with BSMV:*PsSOD1* showed

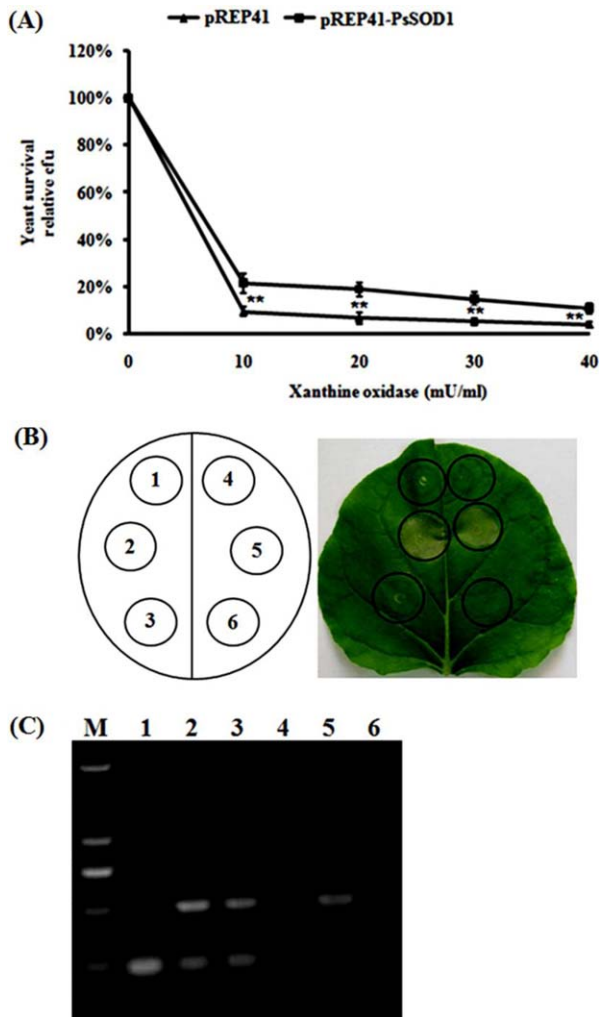


**Fig. 6.** Overexpression of *PsSOD1* in different heterologous systems.

A. *PsSOD1* protects *S. pombe* cells from exogenous superoxide in vitro. Yeasts were incubated in increasing amounts of superoxide generated by addition of increasing amounts of xanthine oxidase to hypoxanthine. The *S. pombe* wild-type JM837 individually carrying pREP41 and pREP41-*PsSOD1* was incubated for 4 h at 37°C, and viable colony forming units (cfu) were determined. The results are plotted as relative yeast survival compared with viable cfu of yeasts incubated in the absence of superoxide (0 mU/ml xanthine oxidase). The results represent the mean from three replicate challenges per strain. Asterisks indicate significant differences (\*\* $P < 0.01$ ) compared with the control.

B. Transient expression of *PsSOD1* in *N. benthamiana*. Tobacco leaves were infiltrated with *A. tumefaciens* cells carrying *PsSOD1*, an empty vector or Bax alone (circles 1, 4, 5), co-infiltrated with *A. tumefaciens* cells individually carrying *PsSOD1* and Bax (circles 2), or infiltrated with *A. tumefaciens* cells carrying *PsSOD1* and followed 24 h later by a second infiltration of *A. tumefaciens* cells carrying Bax (circles 3). Photos were taken from 3 to 6 days after the second infiltration. 1, *PsSOD1*; 2, *PsSOD1* + Bax (co-infiltration); 3, *PsSOD1* + Bax (infiltration 24 h later); 4, empty vector; 5, Bax; 6, MgCl<sub>2</sub>.

C. RT-PCR analysis of *Bax* and *PsSOD1* expression levels in plant tissues treated as described in (B). Total RNA was extracted 60 h after the second infiltration.

greatly increased resistance to the CYR32 isolate, and fewer uredia were formed compared with the control (Fig. 7B). In addition, the plants inoculated with BSMV:*PsSOD1*-as1 and BSMV:*Ta-PsSOD1*-as2 (Supporting Information Fig. S6) showed a similar phenotype, demonstrating that the silencing was specific (Fig. 7B).

To test whether the observed reduction in sporulation was correlated with mycelial growth in the host tissue, fungal biomass measurements were conducted on the infected leaves. Total DNA was extracted from the BSMV-*PsSOD1* inoculated leaves superinfected with *Pst*, and the relative levels of the *Pst* gene *PstEF1* and the wheat gene *TaEF-1a* were quantified using real-time PCR based on the constructed standard curves (Supporting Information Fig. S7). At 15 d after *Pst* inoculation of the leaves infected by BSMV:*PsSOD1*-as1 and BSMV:*PsSOD1*-as2, the fungal biomass was significantly reduced by 37% and 33%, respectively, compared with the controls inoculated with BSMV:γ (Fig. 7C). This result indicated that fungal development was impeded, probably as a result of the virulence penalty imposed by silencing of the targeted fungal genes.

To clarify whether *PsSOD1* was successfully silenced, qRT-PCR was performed to measure the relative transcript level of *PsSOD1* in the fourth leaves infected with *Pst*. The *PsSOD1* transcript in BSMV:*PsSOD1*-as1-infected leaves was reduced by 45%, 80%, and 57% at 24, 48, and 120 hpi with CYR32, respectively; in leaves inoculated with BSMV:*PsSOD1*-as2, the *PsSOD1* transcript was reduced by 58%, 64%, and 41%, respectively, compared with BSMV:γ-infected wheat leaves (Fig. 7D). These results indicate that the expression of *PsSOD1* was significantly reduced via BSMV-HIGS.

#### *HIGS of PsSOD1 impairs fungal growth and increases H<sub>2</sub>O<sub>2</sub> accumulation in the wheat-Pst compatible interactions*

To determine how *PsSOD1* is involved in *Pst* pathogenicity, we assessed the fungal development and host response in HIGS plants inoculated with *Pst*. At 24 hpi, the number of hyphal branches, haustorial mother cells and haustoria in the wheat seedlings inoculated with BSMV:*PsSOD1*-as1 and BSMV:*PsSOD1*-as2 were similar ( $P > 0.05$ ) to those of the control (Supporting Information Fig. S8A); however, hyphal length was clearly reduced (Fig. 8A and F; Supporting Information Fig. S8B). At 48 hpi, the number of hyphal branches, haustorial mother cells and haustoria and hyphal length were significantly decreased (Fig. 8B, G, K and L). Furthermore, the formation of secondary hyphae was significantly limited in the HIGS plants compared with the control at 48 hpi (Supporting Information Fig. S8C). However, with the progression of the *Pst* infection process, there was no difference in colony size at 72 hpi (Supporting Information Fig. S8C), and the infection area was twice as

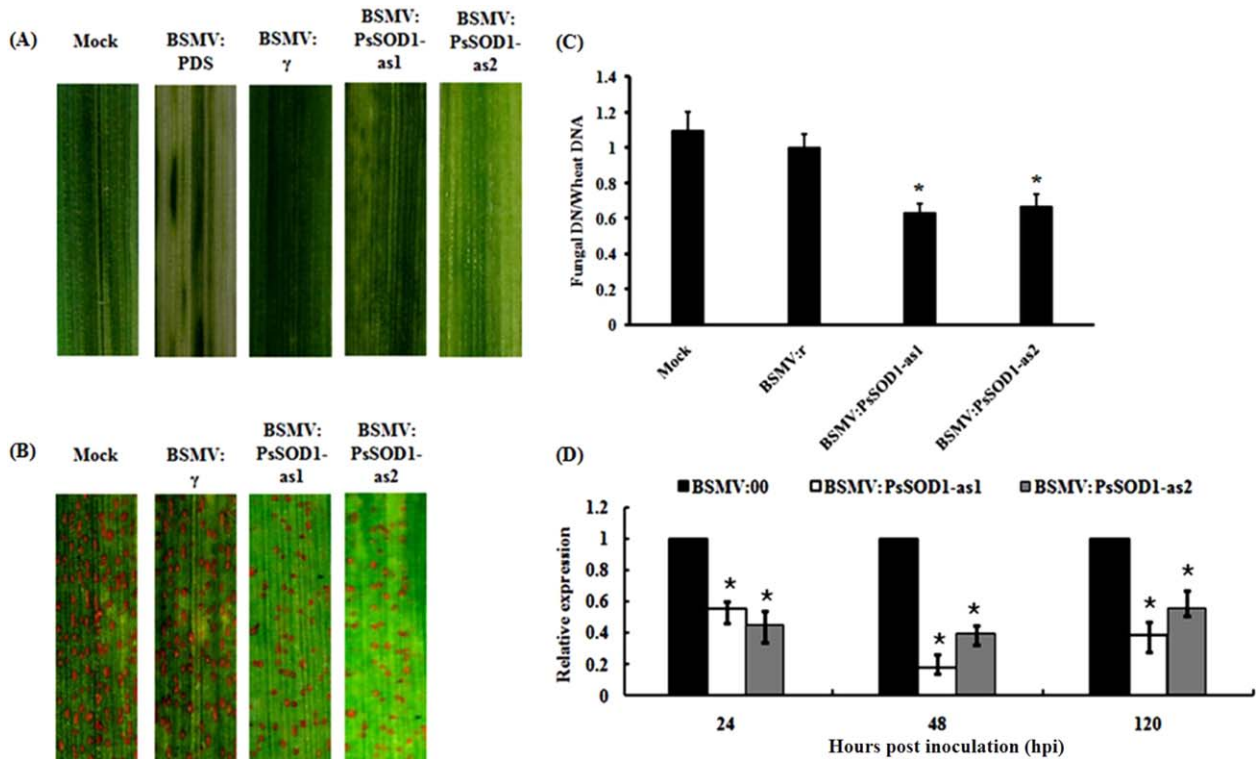


**Fig. 7.** Silencing of *PsSOD1* in the wheat-*Pst* interaction using HIGS leads to reduced virulence. The mean  $\pm$  SD from three independent samples is presented. Asterisks indicate a significant difference ( $P < 0.05$ ) using Student's *t*-test.

A. Mild chlorotic mosaic symptoms were observed on the fourth leaves of seedlings at 9 dpi with BSMV, and bleaching was evident on the fourth leaves of plants infected by BSMV:*TaPDS*. CK, wheat leaves inoculated with FES buffer.

B. Disease phenotypes of the fourth leaves pre-inoculated with BSMV and then challenged with CYR32.

C. Fungal biomass measurements using real-time PCR analysis of total DNA extracted from the wheat leaves infected by CYR32 at 15 dpi. Ratio of total fungal DNA to total wheat DNA was assessed using the wheat gene *TaEF-1a* and the *Pst* gene *PstEF1*.

D. Silencing efficiency assessment of *PsSOD1* in *Pst*. Wheat leaves inoculated with BSMV: $\gamma$  and sampled after inoculation with CYR32 were used as the controls. The data were normalized to the expression level of *TaEF-1a*.

large in the HIGS plants as the control at 120 hpi (Fig. 8C, H and M). However, uredia size was unchanged, so here we observed an unusual overgrowth of hyphae.

To analyse the host response,  $H_2O_2$  accumulation was detected using DAB staining. The results showed that  $H_2O_2$  accumulation was approximately 18-fold higher in the wheat seedlings inoculated with BSMV:*PsSOD1-as1* and BSMV:*PsSOD1-as2* than the control plants at 24 hpi in the compatible interaction (Fig. 8D and I; Supporting Information Fig. S8D). At 48 hpi,  $H_2O_2$  accumulation in the HIGS plants was more than four times higher than that of the control plants. (Fig. 8E, J and N).

## Discussion

Although SODs are known to play an important role in ROS scavenging, few studies have addressed the role of this gene in plant-pathogen interactions. In the present study, a Zn-only SOD gene from *Pst* (*PsSOD1*) was cloned for the first time, and its expression and secretion were

characterized during *Pst* infection of wheat. Furthermore, the function of *PsSOD1* was identified via heterologous expression and a BSMV-HIGS system in the wheat-*Pst* interaction. The results indicate that *PsSOD1* is a novel SOD specific to stripe rust fungi and contributes to *Pst* protection against host-derived oxidative stress.

Cu/Zn-SOD was the first antioxidant enzyme to be characterized. Most Cu/Zn-SODs share a signature motif related to the active site (a copper-binding site and a zinc-binding site) (Zelko *et al.*, 2002). Recently, a Cu-only SOD that lacks a zinc site was identified (Gleason *et al.*, 2014). In the present study, *PsSOD1* was cloned from *Pst*, and the protein encoded by *PsSOD1* exhibited the greatest similarity to Cu/Zn-SODs from other fungi. It was determined that *PsSOD1* is likely a Cu/Zn-SOD. Further domain analysis revealed that this protein only contains the zinc-binding site without the copper-binding site, which differs from the previously identified Cu/Zn-SODs in other species, suggesting that *PsSOD1* potentially encodes a novel SOD.

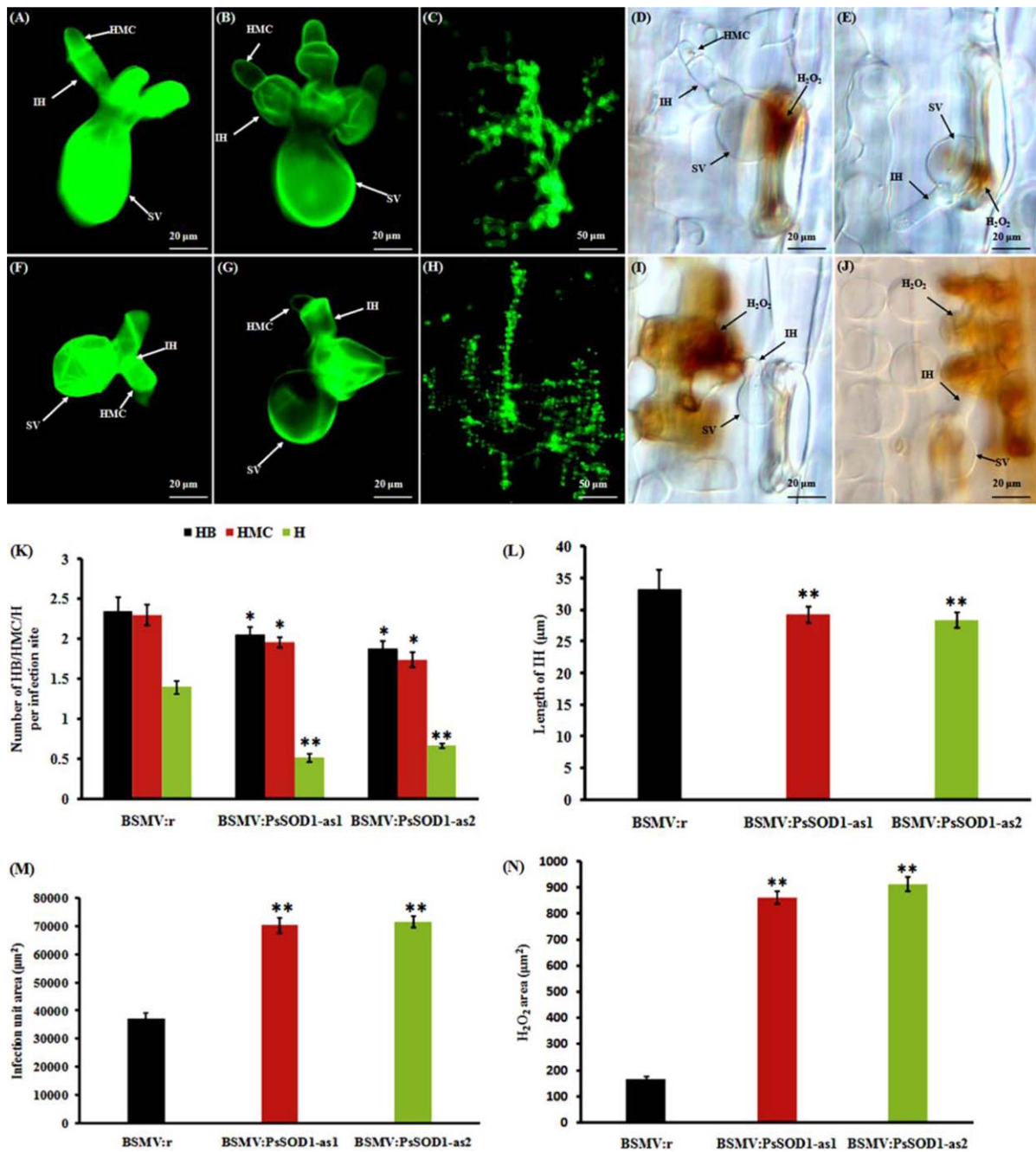


**Fig. 8.** Histological observation of fungal growth and host response in wheat infected by BSMV:γ and recombinant BSMV after inoculation with CYR32. A–E. Fungal growth at 24 hpi (A) or 48 hpi (B), infection unit area at 120 hpi (C), H<sub>2</sub>O<sub>2</sub> accumulation at 24 hpi (D) or 48 hpi (E) in BSMV:γ-infected plants.

F–J. Fungal growth at 24 hpi (F) or 48 hpi (G), infection unit area at 120 hpi (H), H<sub>2</sub>O<sub>2</sub> accumulation at 24 hpi (I) or 48 hpi (J) in BSMV:PsSOD1-infected plants, H<sub>2</sub>O<sub>2</sub> accumulation was calculated using DAB staining.

K. The average number of HB, HMC and H decreased significantly in HIGS plants infected by CYR32.

L. Hyphal length, which is the average distance from the junction of the substomatal vesicle and the hypha to the tip of the hypha, was clearly decreased in HIGS plants infected by CYR32.

M. The infection unit area at 120 hpi per infection unit was significantly increased in HIGS plants infected by CYR32.

N. A significant increase in ROS accumulation was observed in CYR32-infected HIGS plants at 48 hpi. Values represent the means ± standard errors of three independent samples. Differences were assessed using Student's *t*-tests. Asterisks indicate  $P < 0.05$ . SV, substomatal vesicle; HMC, haustorial mother cell; IH, infection hypha; HB, hyphal branch; H, haustoria.

To confirm this finding, the function of *PsSOD1* was identified through complementation of the *S. cerevisiae* *SOD1* mutant. Compared with the control, the complemented strain CS-1 exhibited increased growth rates and higher resistance to menadione. These results indicate that the expression of *PsSOD1* in *S. cerevisiae* could complement the defects observed in the *SOD1* mutant. Thus, PsSOD1 and SOD1 display identical functions during this process, which confirmed that the coding product of *PsSOD1* is a SOD. In addition, PsSOD1 was biochemically characterized. We found that  $Zn^{2+}$  in the reaction significantly increased the enzymatic activity of PsSOD1, but addition of  $Cu^{2+}$  had no effect on enzymatic activity, which is consistent with the bioinformatics prediction of PsSOD1. These results further indicate that PsSOD1 is a Zn-only SOD.

Cu/Zn-SODs are widely distributed in the cytoplasm (Fink and Scandalios, 2002), nucleus (Chang *et al.*, 1988), the intermembrane space of mitochondria (Sturtz *et al.*, 2001) and peroxisomes (Keller *et al.*, 1991). In addition, many species have an extracellular Cu/Zn-SOD. Currently, extracellular Cu/Zn-SODs from yeast, nematodes (*C. elegans*, *C. briggsae*, and *Haemonchus contortus*), crustaceans (blue crab, crayfish), and vertebrates (human, rabbit, mouse, rat, pufferfish) have been identified (Landis and Tower, 2005). In this study, PsSOD1 was predicted to be a secreted protein. To confirm this hypothesis, the predicted signal peptide of PsSOD1 was identified using a yeast secretion system. The results showed that the signal peptide of PsSOD1 was functional, demonstrating that PsSOD1 is a secreted protein.

In addition, numerous studies have reported that Cu/Zn-SOD generally exists as a homodimer or homotetramer (Zeinali *et al.*, 2015). To further confirm secretion and polymerization of PsSOD1 in vivo, apoplastic proteins from uninfected and *Pst*-infected wheat leaves were immunoblotted with an anti-PsSOD1 antibody. Interestingly, the specific band (approximately two times higher than that of a PsSOD1 monomer in molecular weight) was observed when the apoplastic proteins from the *Pst*-infected leaves were separated using native PAGE, whereas the specific band similar to the PsSOD1 monomer in molecular weight appeared when apoplastic proteins from *Pst*-infected leaves were separated in the SDS-PAGE gels. Therefore, we speculate that the secreted PsSOD1 potentially forms a dimer in the apoplastic fluids of wheat leaves. Subsequent BiFC experiments confirmed that PsSOD1 could interact with itself, further validating the dimerization of PsSOD1. These results are consistent with previous studies in other species, such as *E. coli* (Wintjens *et al.*, 2008), *Salmonella enterica* (Ammendola *et al.*, 2008), *C. albicans* (Fr alle *et al.*, 2005) and humans (McCord and Fridovich, 1969).

Previous reports have shown that the expression of Cu/Zn-SODs can be dramatically regulated by various physiological changes and stress conditions. Cu/Zn-SOD mRNA levels are elevated in response to a wide array of mechanical, chemical, and biological stressors, such as heat shock (Hass and Massaro, 1988), shear stress (Inoue *et al.*, 1996), UVB and X-ray irradiation (Yamaoka *et al.*, 1994; Isoherranen *et al.*, 1997), nitric oxide (Frank *et al.*, 2000), ozone (Rahman *et al.*, 1991), and hydrogen peroxide (Yoo *et al.*, 1999). In the present study, we found that *PsSOD1* expression was significantly up-regulated from 12 to 48 hpi. During *Pst* infection of wheat, ROS accumulation generally peaks at 24 hpi (Wang *et al.*, 2007). However,  $O_2^-$  and  $H_2O_2$  generation is seldom detected in the wheat-*Pst* compatible interactions (Wang *et al.*, 2007), implying that *Pst* has a set of effective defence components to scavenge ROS. Thus, it is reasonable that the expression of *PsSOD1* was up-regulated before 48 hpi because PsSOD1 is used for scavenging host-derived ROS in the early stage of infection, which promotes infection of *Pst* by removing ROS stress. In the later stage, ROS could still be detected (Wang *et al.*, 2007; Cheng *et al.*, 2015). These observations led to questions regarding ROS quenching during this period. Voegel  *et al.* (2005) and Link *et al.* (2005) established the idea that rust fungi use the sugar alcohols mannitol and arabitol for ROS quenching because they found that mannitol and arabitol increased dramatically in *Vicia faba* leaves infected with *Uromyces fabae* in the later infection stage and that mannitol and arabitol were sufficient to suppress ROS. Therefore, it is a rational inference that ROS clearance during *Pst* infection is dependent on SOD in the early stage and later is attributed to sugar alcohols.

Numerous studies have demonstrated that up-regulation of Cu/Zn-SOD expression can enhance resistance to oxidative stress in *Histoplasma* (Youseff *et al.*, 2012), *S. cerevisiae* (Fabrizio *et al.*, 2003) and *Drosophila melanogaster* (Orr and Sohal, 1994). In the present study, *PsSOD1* was overexpressed in *S. pombe* treated with exogenous superoxide. Consistent with previous findings, overexpression of *PsSOD1* enhanced *S. pombe* resistance to exogenous superoxide, indicating that PsSOD1 can be secreted from the *S. pombe* cells and scavenge exogenous ROS. Similarly, *PsSOD1* may play important roles in the wheat-*Pst* interactions by eliminating host-derived oxidative stress. In addition, *PsSOD1* overexpression in tobacco significantly suppressed bax-induced cell death. Therefore, we speculate that overexpression and secretion of *PsSOD1* favour *Pst* infection. On the one hand, ROS quenching in the host-pathogen interface could reduce damage to *Pst* itself. On the other hand, *Pst* is a biotrophic fungus that is dependent on the live host. Scavenging ROS may protect host cells from HR-like cell death,

which ensures the smooth progression of nutrient uptake in *Pst*.

SODs are important virulence factors in nearly all pathogenic fungi (Hwang *et al.*, 2002; Cox *et al.*, 2003; Narasipura *et al.*, 2003; Lambou *et al.*, 2010). For example, SOD1 from *C. albicans* and *C. neoformans* directly participates in fungal pathogenicity. Killing of mutant SOD1 cells by macrophages is enhanced in vitro, and fungal virulence is greatly attenuated in vivo (Cox *et al.*, 2003; Narasipura *et al.*, 2003). Disruption of *C. neoformans* SOD1 leads to decreased expression of many *Cryptococcus*-specific virulence factors, including laccase, urease and phospholipase (Cox *et al.*, 2003). In the present study, we used a BSMV-HIGS approach to determine the role of *PsSOD1* in the wheat-*Pst* interaction. The reduced disease symptoms in HIGS wheat seedlings infected by CYR32 suggested that the suppression of *PsSOD1* could reduce the virulence of *Pst*. In addition, H<sub>2</sub>O<sub>2</sub> accumulation was significantly increased, and the fungal development was impeded. Previous studies have shown that ROS, especially H<sub>2</sub>O<sub>2</sub>, act as antimicrobial agents during the plant defence response (Shetty *et al.*, 2008). For example, micromolar concentrations of H<sub>2</sub>O<sub>2</sub> inhibit spore germination of a number of fungal pathogens in vitro (Peng and Kuc, 1992). A concentration of 0.1 mM H<sub>2</sub>O<sub>2</sub> was shown to completely inhibit the growth of cultured bacteria *Pectobacterium carotovorum* subsp. *carotovorum* and result in >95% inhibition of *Phytophthora infestans* growth (Wu *et al.*, 1995). Shetty *et al.* (2007) used in vitro experiments to show that 5 mM H<sub>2</sub>O<sub>2</sub> could inhibit the development of an inoculum from 4-day-old *Septoria tritici* cultures, whereas a concentration of approximately 50 mM was required to inhibit an inoculum from 16-day-old cultures. Thus, we concluded that H<sub>2</sub>O<sub>2</sub> accumulation at the host-pathogen interface in HIGS plants could restrict fungal development during *Pst* infection, resulting in a reduction in the number of uredia.

Although the spread of the secondary hyphae was limited in the early stage of *Pst* infection, the hyphae grew faster with the progression of *Pst* infection. The average infection area per infection site in the HIGS plants was more than twice as high as that of the control at 120 hpi. However, uredia did not grow better. Increasing evidence has suggested that oxidative damage may be a key factor of ageing in species ranging from *C. elegans* to *Drosophila* to humans (Stadtman, 1992; Wallace, 1999; Finkel and Holbrook, 2000; Hekimi and Guarente, 2003). Furthermore, oxidative stress can also cause fungal degeneration, resulting in several changes, including the overgrowth of hyphae, formation of sectors and reduced sporulation and virulence (Li *et al.*, 2014). In the HIGS plants, ROS were significantly accumulated and caused damage to *Pst*. Thus, we infer that abnormal growth of hyphae may be due to *Pst* degeneration caused by ROS stress.

In conclusion, the present study revealed a key role of *PsSOD1* during *Pst* infection. In the wheat-*Pst* compatible interaction, highly expressed *PsSOD1* was secreted into the host-pathogen interface, contributing to *Pst* infection by scavenging ROS derived from the host and suppressing host cell death.

## Experimental Procedures

### Plant materials, strains and culture conditions

The wheat cultivar Suwon 11 (Su11) and the *Pst* pathotype CYR32 (virulent to Su11) were used in the wheat-*Pst* interaction study. Plant cultivation and inoculation with *Pst* were performed as described previously (Kang *et al.*, 2002). To study the *PsSOD1* expression levels in wheat leaves infected by CYR32, urediniospores of CYR32 and leaf tissues were sampled at 0, 6, 12, 18, 24, 36, 48, 72, 120, 168 and 264 h post-inoculation (hpi). *N. benthamiana*, which was used for transient expression, was grown at 25°C with a light regime of 16 h light/8 h darkness.

The strains used in this study are listed in Supporting Information Table S2. *A. tumefaciens* was cultured at 30°C, *E. coli* at 37°C, and *S. cerevisiae* and *S. pombe* at 28°C, all in growth chambers in the dark.

### RNA extraction and qRT-PCR

Total RNA was extracted using RNAiso Reagent (TaKaRa, Tokyo, Japan) according to the manufacturer's instructions. Potential genomic DNA was digested with DNase I. First-strand cDNA was synthesized using a GoScript™ Reverse Transcription System (Promega, Madison, WI) with an oligo(dT)18 primer.

The transcript levels of *PsSOD1* were measured at different developmental stages of the *Pst* infection process by qRT-PCR according to the procedure described by Cheng *et al.* (2015). Elongation factor-1 (EF-1) was used as the endogenous reference to normalize the gene expression in *Pst* (Yin *et al.*, 2009). Each reaction was carried out in triplicate, and three non-template controls were included in the experiment. The specificity of the amplicon was verified at the end of the PCR run using dissociation curve analysis. Two parameters, i.e., a relative quantity of RNA at least twofold higher or lower than the controls and  $P \leq 0.005$ , were used to assess the significance of the differences between time points.

The primers used for qRT-PCR are listed in Supporting Information Table S2.

### Cloning of *PsSOD1*, domain prediction, sequence alignment and polymorphism analysis

To clone the *PsSOD1* gene, primers (Supporting Information Table S2) were designed based on the *PsSOD1* cDNA sequence containing the complete ORF with the wheat-*Pst* interaction cDNA library (Ma *et al.*, 2009). The *PsSOD1* gene was PCR-amplified using a CYR32-infected Su11 cDNA sample as a template. The physicochemical properties of the amino acid sequence of *PsSOD1* were determined using the ProtParam tool of ExPASy (<http://www.expasy.org>). The

protein domain structure was predicted on the basis of Pfam analysis (<http://pfam.sanger.ac.uk/>). The signal peptides of PsSOD1 were then predicted using SignalP 4.1 (<http://www.cbs.dtu.dk/services/SignalP/>). Finally, the amino acid sequence was analysed using BLASTP and compared with non-redundant databases (National Center for Biotechnology Information, NCBI) to identify homologous proteins. Some homologous proteins from other fungi were selected and further compared using ClustalW (version 1.8) multi-alignment software. Then, MEGA5 was used for phylogenetic analysis by the neighbour-joining method.

To identify gene polymorphisms, we compared the coding regions of PsSOD1 among five sequenced *Pst* isolates, including the Chinese CYR32 isolate, three US isolates (PST21, PST43 and PST130) and a UK isolate (PST87-7). To determine nucleotide substitutions in PsSOD1, local BLAST searches using BioEdit software (<http://www.mbio.ncsu.edu/BioEdit/bioedit.html>) were carried out to obtain the corresponding sequences, and DNAMAN software was used to create multiple sequence alignments. At each nucleotide position in the alignment, if there were different bases (one or more) compared with CYR32, one nucleotide substitution was counted. This count was then summed over all positions in the gene.

#### Plasmid construction

To identify the function of PsSOD1, the ORF of PsSOD1 without the signal peptide sequences was amplified and inserted into the *NotI/BamHI* restriction sites in plasmid pDR195 to obtain the complementation construct pDR195-PsSOD1.

For biochemical characterization of PsSOD1, the coding region sequences without a signal peptide were amplified and inserted into the *BamHI/NotI* restriction sites of vector pGEX-4T-1 to generate the recombinant plasmid pGEX-4T-1-PsSOD1.

Functional identification of the predicted signal peptide of PsSOD1 was performed with a yeast secretion system (Jacobs *et al.*, 1997). The yeast signal trap vector pSUC2T7-M13ORI (pSUC2), which carries a truncated invertase, SUC2, lacking both its initiation methionine and signal peptide, was used. DNA fragments encoding the predicted signal peptide of PsSOD1, the identified secretion protein Avr1b (the positive control) and Mg87 without a signal peptide (the negative control) (Gu *et al.*, 2011) were inserted into the *EcoRI/XhoI* restriction sites of vector pSUC2, respectively.

For overexpression in *S. pombe*, the vector pREP41 (Craven *et al.*, 1998) was used. The PsSOD1 amplicon and the pREP41 vector were digested with the restriction enzymes *NdeI* and *BamHI* and then ligated to generate the recombinant plasmid pREP41-PsSOD1.

To determine whether PsSOD1 forms a polymer, the ORF of PsSOD1 without the signal peptide was inserted into the *BamHI/XhoI* restriction sites in vector pSPYNE(R)173 (Waadt *et al.*, 2008) and the *Clal/XhoI* restriction sites in plasmid pSPYCE(M) (Waadt *et al.*, 2008) to generate the recombinant plasmids pSPYNE(R)173-PsSOD1 and pSPYCE(M)-PsSOD1, respectively.

For overexpression of PsSOD1 in tobacco, the ORF of PsSOD1 without a signal peptide and the *Bax* gene were

PCR-amplified and inserted into the *Clal/EcoRI* restriction sites in vector potato virus X (PVX) to construct the recombinant plasmids PVX-PsSOD1 and PVX-Bax, respectively.

A BSMV  $\gamma$  RNA-based vector was constructed as previously described by Holzberg *et al.* (2002). To ensure the specificity of the gene silencing, the fragments that showed the highest polymorphism within this gene family and the lowest sequence similarity with other *Pst* and wheat genes in a BLASTN search of the National Center for Biotechnology Information database were chosen to construct the  $\gamma$  RNA-based derivative plasmids. Consequently, two cDNA fragments derived from the coding region and the 5' untranslated region (UTR) (216 bp, nucleotides 217–432) and from the coding sequence and the 3' UTR (202 bp, nucleotides 833–1034) were used to construct the recombination plasmids PsSOD1-as1 and PsSOD1-as2, respectively, in an antisense orientation.

The primers for all plasmid constructions are listed in Table S2.

#### Complementation of the *S. cerevisiae* Y06913 mutant with PsSOD1

For the *S. cerevisiae* complementation assays, pDR195 and pDR195-PsSOD1 were transformed into the SOD1-deficient strain Y06913 using electroporation. The transformants were selected on SC media without uracil at 28°C. The putative transformants carrying the vector pDR195-PsSOD1 were confirmed using PCR analysis. The function of PsSOD1 was identified based on the growth rate of the positive transformants in SC media with the indicated carbon sources. Growth was monitored in SC with different carbon sources as previously described by Longo *et al.* (1996).

In addition, the complemented strain carrying the recombinant pDR195-PsSOD1 plasmid was used to assay sensitivity to menadione, (2-methylnaphthalene-1,4-dione), an endogenous superoxide-generating compound. Yeast cells grown in SC without uracil were standardized to  $1 \times 10^7$  cells/ml. Five microlitre volumes of a 10-fold dilution series prepared from this suspension were spotted on the surface of SC agar plates containing 0, 0.5, 1 and 2 mM menadione. The plates were incubated for 48 h at 28°C, and growth was observed during the incubation. The  $\Delta$ SOD1 mutant carrying an empty pDR195 vector was used as the control.

#### Expression of GST-tagged fusion proteins and antibody generation

The recombinant plasmid pGEX-4T-1-PsSOD1 was used to transform *E. coli* BL21(DE3)plysS grown in LB medium supplemented with ampicillin (100 mg/l) at 37°C. Protein expression was induced at an  $A_{600}$  of 0.6 by addition of 1.0 mM IPTG for 10 h. The harvested cells were suspended in Tris-HCl buffer (20 mM Tris-HCl; pH 7.9) and lysed by sonication. The supernatant containing the soluble proteins was collected by centrifugation at 12,000 rpm for 15 min and analysed by SDS-PAGE followed by staining with Coomassie brilliant blue.

Purification of the fusion proteins was performed using GSTrap 4B (GE). The GST tag was removed by thrombin

cleavage. Antibodies were obtained by repeated injection of rabbits with the PsSOD1 protein.

#### SOD activity assay

SOD activity was assayed using a photochemical method based on the reduction of nitroblue tetrazolium (NBT). The 3 ml reaction mixture contained 39 mM L-methionine, 225  $\mu$ M nitroblue tetrazolium (NBT), 8  $\mu$ M riboflavin, 30  $\mu$ M EDTA- $\text{Na}_2$ , and 10  $\mu$ l purified enzyme in 50 mM potassium phosphate buffer (pH 7.8). The reaction was initiated by illuminating the reaction mixture for 20 min, and photochemically produced superoxide reacted with NBT. Absorbance of formazan, the product of NBT reduction, was then recorded at 560 nm. One unit of SOD activity was defined as the amount of enzyme that caused 50% of the maximum inhibition of NBT reduction. All assays were performed in triplicate, and average values were reported. Total protein content was measured as described by Lowry *et al.* (1951) using bovine serum albumin as the standard.

The thermal and pH stabilities of the purified enzyme were assessed after the enzyme solution samples were incubated at 20 to 70°C and pH 5 to 13 for 30 min, respectively. The residual activity of each sample was determined after the 30 min reaction. The effects of four metal ions (0.5 mM  $\text{Mn}^{2+}$ ,  $\text{Cu}^{2+}$ ,  $\text{Zn}^{2+}$ , or  $\text{Fe}^{3+}$ ) on the SOD activity of the purified PsSOD1 were measured. Enzyme solutions containing each of the tested agents were incubated in 50 mM phosphate buffer (pH 7.8) at 25°C for 30 min and then assayed for residual activity as described above. The metal content of PsSOD1 was determined using graphite furnace atomic absorption spectroscopy (Thermo Electron, USA) after the enzyme was dialyzed extensively in 10 mM phosphate buffer (pH 7.8) containing 1 mM EDTA and then in buffer without EDTA. All assays were repeated three times.

#### Signal peptide validation of PsSOD1

The recombinant plasmid pSUC2-*PsSOD1*, the control plasmid pSUC2-*Avr1b* and pSUC2-*Mg87* were transformed into the yeast strain YTK12 as previously described by Gietz *et al.* (1995), respectively. All transformants were confirmed by PCR using specific primers. Transformants were grown on yeast minimal medium with sucrose instead of glucose (CMD-W media: 0.67% yeast N base without amino acids, 0.075% tryptophan dropout supplement, 2% sucrose, 0.1% glucose, and 2% agar). To assess invertase secretion, colonies were transferred onto YPRAA plates containing raffinose and lacking glucose (1% yeast extract, 2% peptone, 2% raffinose, and 2 mg/ml antimycin A). The YTK12 strain transformed with the pSUC2 vector encoding the truncated invertase, and the untransformed YTK12 strain were used as negative controls.

#### Preparation of vacuum infiltrate samples and immunoblot analysis

For apoplast protein extraction, a vacuum infiltration procedure was used according to the method described by Dani *et al.* (2005). Uninfected and *Pst*-infected wheat leaf tissues at 48 hpi were excised, washed in chilled  $\text{H}_2\text{O}$  (4°C) and then

submerged in chilled vacuum infiltration buffer (50 mM phosphate buffer, 200 mM NaCl, pH 7.5) in a modified vacuum desiccator. A vacuum of 80 kPa was applied for 10 min using a vacuum pump (KNF Neuberger, Freiburg, Germany) to remove the gas from the apoplastic spaces; during evacuation, the container was periodically shaken to dislodge air bubbles from the leaf surfaces. Following the gradual release of the vacuum, leaf strips were blotted dry. The extract was centrifuged in VectaSpin tubes with polypropylene mesh inserts (Whatman International, Maidstone, UK) at  $900 \times g$  for 10 min at 4°C. The vacuum infiltrate (VI) was collected in the bottom of the tubes, dialyzed against  $\text{H}_2\text{O}$  overnight at 4°C, and then resuspended in a small volume of water or buffer before use.

For the western blot analysis, apoplastic proteins from *Pst*-infected wheat leaves were separated using native PAGE or SDS-PAGE and transferred onto nitrocellulose membranes. The blot was blocked with 5% skim milk in TBS buffer (10 mM Tris-HCl buffer containing 150 mM NaCl; pH, 7.5) for 2 h at room temperature. The samples were then incubated with the anti-PsSOD1 antibody (1:500) in 2% skim milk/TBS overnight at 4°C, washed with TBS containing 0.1% Tween-20 (TBST), and finally reacted with goat anti-rabbit IgG horseradish peroxidase (HRP) (1:500) for 2 h at 25°C. After incubation and washing, the nitrocellulose membrane was immunostained with 3,3'-diaminobenzidine (DAB) for 10 min in the dark. Apoplastic proteins from uninfected wheat leaves and purified GST-PsSOD1 fusion proteins were used as controls.

#### Split GFP assay

nYFP sequences were fused to the N-terminal sequences of PsSOD1 in the vector pSPYNE(R)173, and cYFP sequences were fused to the C-terminal sequences of PsSOD1 in the plasmid pSPYCE(M). The fusion proteins were introduced into *N. benthamiana* leaves using the *Agrobacterium*-mediated transient expression method (Xuan *et al.*, 2013). Interactions of the co-expressed proteins were monitored by detecting YFP fluorescence using a Zeiss LSM510 META confocal microscope. All assays were repeated independently at least three times with comparable results.

#### Overexpression of PsSOD1 in *S. Pombe*

To determine the role of PsSOD1 in resisting exogenous superoxide, the complete ORF of *PsSOD1* was introduced into the overexpression vector pREP41, and the recombinant plasmid pREP41-*PsSOD1* was transformed into the wild-type *S. pombe* JM837 by electroporation. The transformants were selected on SC media without leucine at 28°C and validated using PCR. The positive transformant was cultured and collected from log-phase liquid cultures. Cells ( $1 \times 10^5$ ) were incubated in a superoxide-generating system consisting of 50 mM Tris pH 8, 100 mM hypoxanthine, and increasing amounts of xanthine oxidase (X4500; Sigma) in a total volume of 500 ml. Yeast cultures were incubated for 4 h at 28°C with shaking (200 rpm) in a humidified chamber. After incubation, the yeast cultures were removed, and serial dilutions were plated on solid media to identify viable fungal colony forming units (cfu). The JM837 strain carrying the empty pREP41

vector was used as the negative control. Survival was statistically compared between strains using one-tailed Student's *t*-tests.

#### Overexpression of PsSOD1 in *N. Benthamiana*

The reconstructed vectors PVX-*PsSOD1*, PVX-*Bax*, and PVX empty vector were transformed individually into *A. tumefaciens* strain GV3101. Infiltration experiments were performed using 4- to 6-week-old tobacco plants. *A. tumefaciens* cell suspensions carrying the transgenes were infiltrated into tobacco leaves as described by Wang *et al.* (2011). At 24 h after the initial infiltration with *A. tumefaciens* carrying PVX-*PsSOD1*, the same infiltration site was challenged with *A. tumefaciens* cell suspensions carrying the *Bax* gene. Empty vector or MgCl<sub>2</sub> was infiltrated in parallel as controls. RT-PCR was used to evaluate the expression of the *PsSOD1* and *Bax* genes in tobacco leaves exposed to different treatments. The infiltrated tobacco leaves were harvested 60 h after the second infiltration, and total RNA was extracted. The development of symptoms was monitored 3 to 6 days after the second infiltration.

The primers used for RT-PCR are listed in Supporting Information Table S2.

#### BSMV-mediated *PsSOD1* gene silencing in the compatible wheat-*Pst* interaction

BSMV-VIGS was carried out as previously described by Cheng *et al.* (2015). To silence *PsSOD1*, two BSMV viruses (BSMV:*PsSOD1*-as1 and BSMV:*PsSOD1*-as2) were used to inoculate wheat seedlings. BSMV:*TaPDS* (*TaPDS*: wheat phytoene desaturase gene) and BSMV:γ were used as controls for the BSMV infection. Mock inoculations were performed with 1 × FES buffer as previously described (Cheng *et al.*, 2015). At least 18 wheat seedlings were used for each assay. BSMV-infected wheat plants were kept in a growth chamber at 23 ± 2°C. The fourth leaves were further inoculated with fresh CYR32 urediniospores at 9 d after virus inoculation, and the plants were then maintained at 18 ± 2°C and sampled at 0, 24, 48, and 120 hpi for qRT-PCR and histological observation (Wang *et al.*, 2007). The silencing efficiency of *PsSOD1* was confirmed using qRT-PCR as described above. The phenotypes of the fourth leaves were observed and photographed at 14 days after pathogen inoculation. Biological replicates were carried out in triplicate.

#### Quantification of *Pst* in inoculated leaves

To measure changes in fungal biomass, relative quantification of the single-copy target genes *PsEF1* and *TaEF1* was carried out (Panwar *et al.*, 2013). Total genomic DNA of the wheat cultivar Su11 or the *Pst* pathotype CYR32 was used to prepare standard curves derived from at least six serial dilutions for each. The correlation coefficients for the analysis of the dilution curves were above 0.99. The relative quantities of the PCR products of *PsEF1* and *TaEF1* in mixed/infected samples were calculated using the gene-specific standard curves to quantify the *Pst* and wheat genomic DNA, respectively.

The primers used are listed in Supporting Information Table S2.

#### Histological observation of fungal growth and host response

To characterize the cellular interaction between wheat and *Pst*, the fungal development and host response were observed microscopically. The leaf segments were fixed and stained as described previously (Wang *et al.*, 2007). The number of hyphal branches, haustorial mother cells and haustoria, hyphal length and spread of hyphal growth were determined as previously described (Cheng *et al.*, 2015). To obtain high-quality images of *Pst* infection structures in wheat leaves, wheat germ agglutinin conjugated to Alexa Fluor-488 (Invitrogen) was used as previously described (Ayliffe *et al.*, 2010).

To detect plant responses, H<sub>2</sub>O<sub>2</sub> accumulation was studied at 24 and 48 hpi using 3,3'-diaminobenzidine (DAB; Amresco, Solon, OH) staining (Wang *et al.*, 2007). Fifty infection sites on five randomly selected leaf segments per treatment were assessed. Standard deviations were determined, and Tukey's test was used for statistical analysis.

#### Acknowledgements

This study was supported by the National Key Basic Research Program of China (2013CB127700), the 111 Project of the Ministry of Education of China (B07049), Chinese Universities Scientific Fund (2452016004), the National Natural Science Foundation of China (No. 31430069), and Natural Science Basic Research Plan in Shaanxi Province of China (2015JM3089).

#### References

- Abreu, I.A., and Cabelli, D.E. (2010) Superoxide dismutases—a review of the metal-associated mechanistic variations. *Biochim Biophys Acta* **1804**: 263–274.
- Ammendola, S., Pasquali, P., Pacello, F., Rotilio, G., Castor, M., Libby, S.J., *et al.* (2008) Regulatory and structural differences in the Cu,Zn-superoxide dismutases of *Salmonella enterica* and their significance for virulence. *J Biol Chem* **283**: 13688–13699.
- Apel, K., and Hirt, H. (2004) Reactive oxygen species: metabolism, oxidative stress, and signal transduction. *Annu Rev Plant Biol* **55**: 373–399.
- Ayliffe, M., Devilla, R., Mago, R., White, R., Talbot, M., Pryor, A., and Leung, H. (2010) Nonhost resistance of rice to rust pathogens. *Mol Plant Microbe Interact* **24**: 1143–1155.
- Briones-Martin-del-Campo, M., Orta-Zavalza, E., Cañas-Villamar, I., Gutiérrez-Escobedo, G., Juárez-Cepeda, J., Robledo-Márquez, K., *et al.* (2015) The superoxide dismutases of *Candida glabrata* protect against oxidative damage and are required for lysine biosynthesis, DNA integrity and chronological life survival. *Microbiology* **161**: 300–310.
- Chang, L.Y., Slot, J.W., Geuze, H.J., and Crapo, J.D. (1988) Molecular immunocytochemistry of the CuZn superoxide dismutase in rat hepatocytes. *J Cell Biol* **107**: 2169–2179.
- Chaves, G.M., Bates, S., Maccallum, D.M., and Odds, F.C. (2007) *Candida albicans* GRX2, encoding a putative glutaredoxin, is required for virulence in a murine model. *Genet Mol Res* **6**: 1051–1063.
- Cheng, Y.L., Wang, X.J., Yao, J.N., Voegelé, R.T., Zhang, Y.R., Wang, W.M., *et al.* (2015) Characterization of protein

- kinase *PsSRPKL*, a novel pathogenicity factor in the wheat stripe rust fungus. *Environ Microbiol* **17**: 2601–2617.
- Cox, G.M., Harrison, T.S., McDade, H.C., Taborda, C.P., Heinrich, G., Casadevall, A., and Perfect, J.R. (2003) Superoxide dismutase influences the virulence of *Cryptococcus neoformans* by affecting growth within macrophages. *Infect Immun* **71**: 173–180.
- Craven, R.A., Griffiths, D.J., Sheldrick, K.S., Randall, R.E., Hagan, I.M., and Carr, A.M. (1998) Vectors for the expression of tagged proteins in *Schizosaccharomyces pombe*. *Gene* **221**: 59–68.
- Dani, V., Simon, W.J., Duranti, M., and Croy, R.R. (2005) Changes in the tobacco leaf apoplast proteome in response to salt stress. *Proteomics* **5**: 737–745.
- Fabrizio, P., Liou, L.L., Moy, V.N., Diaspro, A., Valentine, J.S., Gralla, E.B., and Longo, V.D. (2003) SOD2 functions downstream of Sch9 to extend longevity in yeast. *Genetics* **163**: 35–46.
- Fink, R.C., and Scandalios, J.G. (2002) Molecular evolution and structure function relationships of the superoxide dismutase gene families in angiosperms and their relationship to other eukaryotic and prokaryotic superoxide dismutases. *Arch Biochem Biophys* **399**: 19–36.
- Finkel, T., and Holbrook, N.J. (2000) Oxidants, oxidative stress and the biology of aging. *Nature* **408**: 239–247.
- Frank, S., Kampfer, H., Podda, M., Kaufmann, R., and Pfeilschifter, J. (2000) Identification of copper/zinc superoxide dismutase as a nitric oxide-regulated gene in human (HaCaT) keratinocytes: implications for keratinocyte proliferation. *Biochem J* **346**: 719–728.
- Fréalle, E., Noël, C., Viscogliosi, E., Camus, D., Dei-Cas, E., and Delhaes, L. (2005) Manganese superoxide dismutase in pathogenic fungi: an issue with pathophysiological and phylogenetic involvements. *FEMS Immunol Med Microbiol* **45**: 411–422.
- Fridovich, I. (1978) The biology of oxygen radicals. *Science* **201**: 875–880.
- Fridovich, I. (1995) Superoxide radical and superoxide dismutases. *Annu Rev Biochem* **64**: 97–112.
- Gietz, R.D., Schiestl, R.H., Willems, A.R., and Woods, R.A. (1995) Studies on the transformation of intact yeast cells by the LiAc/SS-DNA/PEG procedure. *Yeast* **11**: 355–360.
- Gleason, J.E., Galaldeen, A., Peterson, R.L., Taylor, A.B., Holloway, S.P., Waninger-Saroni, J., et al. (2014) *Candida albicans* SOD5 represents the prototype of an unprecedented class of Cu-only superoxide dismutases required for pathogen defense. *Proc Natl Acad Sci USA* **111**: 5866–5871.
- Gu, B., Kale, S.D., Wang, Q.H., Wang, D.H., Pan, Q.N., Cao, H., et al. (2011) Rust secreted protein Ps87 is conserved in diverse fungal pathogens and contains a RXLR-like motif sufficient for translocation into plant cells. *PLoS One* **6**: e27217.
- Hass, M.A., and Massaro, D. (1988) Regulation of the synthesis of superoxide dismutases in rat lungs during oxidant and hyperthermic stresses. *J Biol Chem* **263**: 776–781.
- Hekimi, S., and Guarente, L. (2003) Genetics and the specificity of the aging process. *Science* **299**: 1351–1354.
- Holzberg, S., Brosio, P., Gross, C., and Pogue, G.P. (2002) Barley stripe mosaic virus-induced gene silencing in a monocot plant. *Plant J* **30**: 315–327.
- Hwang, C.S., Rhie, G.E., Oh, J.H., Huh, W.K., Yim, H.S., and Kang, S.O. (2002) Copper- and zinc-containing superoxide dismutase (Cu/ZnSOD) is required for the protection of *Candida albicans* against oxidative stresses and the expression of its full virulence. *Microbiology* **148**: 3705–3713.
- Imlay, J.A. (2003) Pathways of oxidative damage. *Annu Rev Microbiol* **57**: 395–418.
- Inoue, N., Ramasamy, S., Fukai, T., Nerem, R.M., and Harrison, D.G. (1996) Shear stress modulates expression of Cu/Zn superoxide dismutase in human aortic endothelial cells. *Circ Res* **79**: 32–37.
- Isoherranen, K., Peltola, V., Laurikainen, L., Punnonen, J., Laihia, J., Ahotupa, M., and Punnonen, K. (1997) Regulation of copper/zinc and manganese superoxide dismutase by UVB irradiation, oxidative stress and cytokines. *J Photochem Photobiol B* **40**: 288–293.
- Jacobs, K.A., Collins-Racie, L.A., Colbert, M., Duckett, M., Golden-Fleet, M., Kelleher, K., et al. (1997) A genetic selection for isolating cDNAs encoding secreted proteins. *Gene* **198**: 289–296.
- Jeong, J.H., Kwon, E.S., and Roe, J.H. (2001) Characterization of the manganese-containing superoxide dismutase and its gene regulation in stress response of *Schizosaccharomyces pombe*. *Biochem Biophys Res Commun* **283**: 908–914.
- Kang, Z.S., Huang, L.L., and Buchenauer, H. (2002) Ultrastructural changes and localization of lignin and callose in compatible and incompatible interactions between wheat and *Puccinia striiformis*. *Zeitschrift Für Pflanzenkrankheiten Und Pflanzenschutz* **109**: 25–37.
- Keller, G.A., Warner, T.G., Steimer, K.S., and Hallewell, R.A. (1991) Cu, Zn superoxide dismutase is a peroxisomal enzyme in human fibroblasts and hepatoma cells. *Proc Natl Acad Sci USA* **88**: 7381–7385.
- Lambou, K., Lamarre, C., Beau, R., Dufour, N., and Latge, J.P. (2010) Functional analysis of the superoxide dismutase family in *Aspergillus fumigatus*. *Mol Microbiol* **75**: 910–923.
- Landis, G.N., and Tower, J. (2005) Superoxide dismutase evolution and life span regulation. *Mech Ageing Dev* **126**: 365–379.
- Li, L., Hu, X., Xia, Y.L., Xiao, G.H., Zheng, P., and Wang, C.S. (2014) Linkage of oxidative stress and mitochondrial dysfunctions to spontaneous culture degeneration in *Aspergillus nidulans*. *Mol Cell Proteomics* **13**: 449–461.
- Link, T., Lohaus, G., Heiser, I., Mendgen, K., Hahn, M., and Voegelé, R.T. (2005) Characterization of a novel NADP<sup>+</sup>-dependent D-arabitol dehydrogenase from the plant pathogen *Uromyces fabae*. *Biochem J* **389**: 289–295.
- Longo, V.D., Liou, L.L., Valentine, J.S., and Gralla, E.B. (1999) Mitochondrial superoxide decreases yeast survival in stationary phase. *Arch Biochem Biophys* **365**: 131–142.
- Longo, V.D., Gralla, E.B., and Valentine, J.S. (1996) Superoxide dismutase activity is essential for stationary phase survival in *Saccharomyces cerevisiae*. *J Biol Chem* **271**: 12275–12280.
- Lowry, O.H., Rosebrough, N.J., Farr, A.L., and Randall, R.L. (1951) Protein measurement with the Folin phenol reagent. *J Biol Chem* **193**: 265–275.
- Ma, J.B., Huang, X.L., Wang, X.J., Chen, X.M., Qu, Z.P., Huang, L.L., and Kang, Z.S. (2009) Identification of

- expressed genes during compatible interaction between stripe rust (*Puccinia striiformis*) and wheat using a cDNA library. *BMC Genomics* **10**: 586.
- Manfredini, V., Roehrs, R., Peralba, M.C., Henriques, J.A., Saffi, J., Ramos, A.L., and Benfato, M.S. (2004) Glutathione peroxidase induction protects *Saccharomyces cerevisiae* *sod1Δ sod2Δ* double mutants against oxidative damage. *Braz J Med Biol Res* **37**: 159–165.
- McCord, J.M., and Fridovich, I. (1969) Superoxide dismutase an enzymic function for erythrocyte (hemocuprein). *J Biol Chem* **244**: 6049–6055.
- Miller, A.F. (2012) Superoxide dismutases: ancient enzymes and new insights. *FEBS Lett* **586**: 585–595.
- Mittler, R. (2002) Oxidative stress, antioxidants and stress tolerance. *Trends Plant Sci* **7**: 405–410.
- Myouga, F., Hosoda, C., Umezawa, T., Iizumi, H., Kuromori, T., Motohashi, R., et al. (2008) Heterocomplex of iron superoxide dismutases defends chloroplast nucleoids against oxidative stress and is essential for chloroplast development in *Arabidopsis*. *Plant Cell* **20**: 3148–3162.
- Narasipura, S.D., Ault, J.G., Behr, M.J., Chaturvedi, V., and Chaturvedi, S. (2003) Characterization of Cu,Zn superoxide dismutase (SOD1) gene knock-out mutant of *Cryptococcus neoformans* var. *gattii*: role in biology and virulence. *Mol Microbiol* **47**: 1681–1694.
- Narasipura, S.D., Chaturvedi, V., and Chaturvedi, S. (2005) Characterization of *Cryptococcus neoformans* variety *gattii* SOD2 reveals distinct roles of the two superoxide dismutases in fungal biology and virulence. *Mol Microbiol* **55**: 1782–1800.
- O'Brien, K.M., Dirmeier, R., Engle, M., and Poyton, R.O. (2004) Mitochondrial protein oxidation in yeast mutants lacking manganese- (MnSOD) or copper- and zinc-containing superoxide dismutase (CuZn-SOD): evidence that MnSOD and CuZnSOD have both unique and overlapping functions in protecting mitochondrial proteins from oxidative damage. *J Biol Chem* **279**: 51817–51827.
- Orr, W., and Sohal, R.S. (1994) Extension of life-span by overexpression of superoxide dismutase and catalase in *Drosophila melanogaster*. *Science* **263**: 1128–1130.
- Panwar, V., McCallum, B., and Bakkeren, G. (2013) Endogenous silencing of *Puccinia triticina* pathogenicity genes through in planta-expressed sequences leads to the suppression of rust diseases on wheat. *Plant J* **73**: 521–532.
- Peng, M., and Kuc, J. (1992) Peroxidase-generated hydrogen peroxide as a source of antifungal activity in vitro and on tobacco leaf disks. *Phytopathology* **82**: 696–699.
- Perez, I.B., and Brown, P.J. (2014) The role of ROS signaling in cross-tolerance from model to crop. *Front Plant Sci* **5**: 754.
- Perry, J.J.P., Shin, D.S., Getzoff, E.D., and Tainer, J.A. (2010) The structural biochemistry of the superoxide dismutases. *Biochim Biophys Acta* **1804**: 245–262.
- Pilon, M., Ravet, K., and Tapken, W. (2011) The biogenesis and physiological function of chloroplast superoxide dismutases. *Biochim Biophys Acta* **1807**: 989–998.
- Priya, B., Premanandh, J., Dhanalakshmi, R.T., Seethalakshmi, T., Uma, L., Prabakaran, D., and Subramanian, G. (2007) Comparative analysis of cyanobacterial superoxide dismutases to discriminate canonical forms. *BMC Genomics* **8**: 10.
- Rahman, I., Clerch, L.B., and Massaro, D. (1991) Rat lung antioxidant enzyme induction by ozone. *Am J Physiol* **260**: 412–418.
- Shetty, N.P., Jørgensen, H.J.L., Jensen, J.D., Collinge, D.B., and Shetty, H.S. (2007) Role of hydrogen peroxide during the interaction between the hemibiotrophic fungal pathogen *Septoria tritici* and wheat. *New Phytol* **174**: 637–647.
- Shetty, N.P., Jørgensen, H.J.L., Jensen, J.D., Collinge, D.B., and Shetty, H.S. (2008) Roles of reactive oxygen species in interactions between plants and pathogens. *Eur J Plant Pathol* **121**: 267–280.
- Stadtman, E.R. (1992) Protein oxidation and aging. *Science* **257**: 1220–1224.
- Sturtz, L.A., Diekert, K., Jensen, L.T., Lill, R., and Culotta, V.C. (2001) A fraction of yeast Cu, Zn-superoxide dismutase and its metallochaperone, CCS, localize to the intermembrane space of mitochondria. *J Biol Chem* **276**: 38084–38089.
- Voegele, R.T., Hahn, M., Lohaus, G., Link, T., Heiser, I., and Mendgen, K. (2005) Possible roles for mannitol and mannitol dehydrogenase in the biotrophic plant pathogen *Uromyces fabae*. *Plant Physiol* **137**: 190–198.
- Waadt, R., Schmidt, L.K., Lohse, M., Hashimoto, K., Bock, R., and Kudla, J. (2008) Multicolor bimolecular fluorescence complementation reveals simultaneous formation of alternative CBL/CIPK complexes in planta. *Plant J* **56**: 505–516.
- Wallace, D.C. (1999) Mitochondrial diseases in man and mouse. *Science* **283**: 1482–1488.
- Wang, C.F., Huang, L.L., Buchenauer, H., Han, Q.M., Zhang, H.C., and Kang, Z.S. (2007) Histochemical studies on the accumulation of reactive oxygen species ( $O_2^{2-}$  and  $H_2O_2$ ) in the incompatible and compatible interaction of wheat–*Puccinia striiformis* f. sp. *tritici*. *Physiol Mol Plant P* **71**: 230–239.
- Wang, Q.Q., Han, C.Z., Ferreira, A.O., Yu, X.L., Ye, W.W., Tripathy, S., et al. (2011) Transcriptional programming and functional interactions within the *Phytophthora sojae* RXLR effector repertoire. *Plant Cell* **23**: 2064–2086.
- Wintjens, R., Gilis, D., and Rooman, M. (2008) Mn/Fe superoxide dismutase interaction fingerprints and prediction of oligomerization and metal cofactor from sequence. *Proteins* **70**: 1564–1577.
- Wu, G.S., Short, B.J., Lawrence, E.B., Levine, E.B., Fitzsimmons, K.C., and Shah, D.M. (1995) Disease resistance conferred by expression of a gene encoding  $H_2O_2$ -generating glucose oxidase in transgenic potato plants. *Plant Cell* **7**: 1357–1368.
- Wuerges, J., Lee, J.W., Yim, Y.I., Yim, H.S., Kang, S.O., and Djinovic Carugo, K. (2004) Crystal structure of nickel-containing superoxide dismutase reveals another type of active site. *Proc Natl Acad Sci USA* **101**: 8569–8574.
- Xie, X.Q., Li, F., Ying, S.H., and Feng, M.G. (2012) Additive contributions of two manganese-cored superoxide dismutases (MnSODs) to antioxidation, UV tolerance and virulence of *Beauveria bassiana*. *PLoS One* **7**: e30298.
- Xuan, Y.H., Hua, Y.B., Chen, L.Q., Sosso, D., Ducat, D.C., Hou, B.H., and Frommera, W.B. (2013) Functional role of oligomerization for bacterial and plant SWEET sugar transporter family. *Proc Natl Acad Sci USA* **110**: E3685–E3694.
- Yamaoka, K., Sato, E.F., and Utsumi, K. (1994) Induction of two species of superoxide dismutase in some organs of rats by low dose X-irradiation. *Physiol Chem Phys Med NMR* **26**: 205–214.

- Yin, C.T., Chen, X.M., Wang, X.J., Han, Q.M., Kang, Z.S., and Hulbert, S.H. (2009) Generation and analysis of expression sequence tags from haustoria of the wheat stripe rust fungus *Puccinia striiformis* f. sp. *tritici*. *BMC Genomics* **10**: 626.
- Yoo, H.Y., Chang, M.S., and Rho, H.M. (1999) The activation of the rat copper/zinc superoxide dismutase gene by hydrogen peroxide through the hydrogen peroxide-responsive element and by paraquat and heat shock through the same heat shock element. *J Biol Chem* **274**: 23887–23892.
- Youseff, B.H., Holbrook, E.D., Smolnycki, K.A., and Rappleye, C.A. (2012) Extracellular superoxide dismutase protects *histoplasma* yeast cells from host-derived oxidative stress. *PLoS Pathog* **8**: e1002713.
- Zeinali, F., Homaei, A., and Kamrani, E. (2015) Sources of marine superoxide dismutases: Characteristics and applications. *Int J Biol Macromol* **79**: 627–637.
- Zelko, I.N., Mariani, T.J., and Folz, R.J. (2002) Superoxide dismutase multigene family: a comparison of the CuZn-SOD (SOD1), Mn-SOD (SOD2), and EC-SOD (SOD3) gene structures, evolution and expression. *Free Radic Biol Med* **33**: 337–349.

### Supporting information

Additional supporting information may be found in the online version of this article at the publisher's web-site:

**Fig. S1.** Prediction of conserved domains (A) and signal peptides (B) of PsSOD1 from Pst. The protein domains and signal peptides of PsSOD1 were predicted using Pfam analysis (<http://pfam.sanger.ac.uk/>) and SignalP 4.1 (<http://www.cbs.dtu.dk/services/SignalP/>), respectively.

**Fig. S2.** Alignment of the amino acid sequences of PsSOD1 with Cu/Zn-SODs from other rust fungi. Alignment was maximized by introducing gaps, which are indicated by dashes. Identical (\*), highly similar (:), and similar (.) amino acids are also indicated. Abbreviations: CYR32, PsSOD1 from the Pst pathotype CYR32; Pg, Cu/Zn-SOD from *P. graminis* f. sp. *tritici* CRL 75-36-700-3 (GenBank accession number XP\_003326013); Ps, Cu/Zn-SOD from *Puccinia sorghi* (GenBank 11 accession number KNZ59826); Mlp, Cu/Zn-SOD from *Melampsora larici-populina* 98AG31 (GenBank accession number XP\_007413252).

**Fig. S3.** Analysis of conserved domains of Cu/Zn-SODs (A) and Cu-only SODs (B). The protein domains were predicted using Pfam analysis (<http://pfam.sanger.ac.uk/>).

**Fig. S4.** Multiple sequence alignment of PsSOD1 from different Pst isolates. Identical (\*) and 16 highly similar amino acids are indicated. Red box: different amino acid substitutions; ▼: Zn binding site; blue line: conserved domain.

**Fig. S5.** A. The native PAGE profiles of the purified GST and GST-PsSOD1 proteins. Lane 1, purified GST proteins; lane 2, purified GST-PsSOD1 fusion proteins; M, marker. B. Western blot analysis of the apoplastic proteins separated in the SDS-PAGE gels. Lane 1, apoplastic proteins from Pst-infected wheat leaves; lane 2, apoplastic proteins from healthy wheat leaves.

**Fig. S6.** Sequence regions for HIGS 1 in this study.

**Fig. S7.** Standard curves generated for the absolute quantification of Pst (A) and wheat (B). Threshold cycles (Ct) are plotted against the initial copy number of template DNA (104, 105, 1063, 107, 108, 109 and 10104). Genomic DNA of the wheat cultivar Su11 or the Pst pathotype CYR32 urediniospores was used to construct the standard curves.

**Fig. S8.** HIGS of PsSOD1 shows limited fungal development and increased ROS accumulation in the host cells at 24 hpi. Values represent the means ± standard errors of three independent samples. Differences were assessed using Student's t-tests. Asterisks indicate  $P < 0.05$ . (A) The average number of hyphal branches (HB), haustorial mother cells (HMC) and haustoria (H) did not differ significantly in CYR32-infected HIGS plants compared with the control. (B) Hyphal length was clearly decreased in CYR32-infected HIGS plants. (C) The infection unit area at 48 hpi per infection unit was significantly decreased in CYR32-infected HIGS plants, whereas there was no difference in the infection unit area at 72 hpi. (D) ROS accumulation increased significantly in CYR32-infected HIGS plants at 24 hpi.

**Table S1.** Overview of intraspecies nucleotide polymorphism in *PsSOD1*.

**Table S2.** Oligonucleotides and strains in this study.